Bifurcation Control of Rotating Stall with Actuator Magnitude and Rate Limits*

Yong Wang
yongwang@cds.caltech.edu
Division of Engineering and Applied Science
California Institute of Technology
Pasadena, California 91125

Simon Yeung†
yeung@crd.ge.com
General Electric Company
Bldg KW, Rm D211
P. O. Box 8
Schenectady, NY 12301

Richard M. Murray
murray@cds.caltech.edu
Division of Engineering and Applied Science
California Institute of Technology
Pasadena, California 91125

Submitted, Automatica

Dec. 26, 1999

Abstract

Nonlinear qualitative analysis is performed on the Moore-Greitzer model to evaluate the tradeoff of fluid noise, actuator magnitude saturation, bandwidth, rate limits, and the shape of compressor characteristics in active control of rotating stall in axial compressors with bleed valve actuators. Model order reduction is achieved by approximating the dynamics on the invariant manifold that captures the bifurcations and instabilities. Bifurcations and qualitative dynamics are obtained by analyzing the reduced system. The operability enhancement is defined as the extension of operating range for which fully developed rotating stall is avoided. Analytic formulas are derived for the operability enhancement as a function of noise level, actuator saturation limits, and the shape of the compressor characteristic, which is the major nonlinearity in the model. The shape of the compressor characteristic, especially the unstable part, is critical to the rate required for robust operability near the peak for the closed loop system. Experiments are carried out on a single-stage low-speed axial compressor using different level of steady air injections to generate different compressor characteristics. The theoretical formulas give good

*Funding for this research was provided in part by AFOSR grant F49620-95-1-0409.

†This work was performed while the author was at the California Institute of Technology.

qualitative estimates to experimental data and simulations using a high fidelity model (37 states).

Key Words-Axial compressors; compressor characteristic; rotating stall; active control; actuator magnitude and rate saturation; operability; bifurcation; center manifold.

1 Introduction

One of the limiting factors of aeroengine performance is aerodynamic instability in the compression system at high loading, typically in the form of rotating stall and surge (see Greitzer (1981) for detailed description). Rotating stall occurs when a nonaxisymmetric flow disturbance develops around the annulus of the compressor and rotates at a fraction of the rotor speed. Once rotating stall develops, the compressor loses pressure rise and typically cannot recover the desired operating condition of steady axisymmetric flow due to the hysteresis. Rotating stall causes drastic reduction in the pressure rise and flow rate of the compressor, overheating on the turbine, and an abrupt drop in the power output of the engine. The unsteady nonaxisymmetric flow in rotating stall exerts periodic loading on the blades and may induce vibrations of the blades, which may cause blade fatigue and structural damage. The flow and pressure drop caused by rotating stall may also induce large amplitude axisymmetric oscillations across the compression system called surge which exerts high level stress to the blades and causes engine failure.

Active control of rotating stall refers to either stabilization of the steady axisymmetric flow past the point of peak pressure rise, which typically requires many actuators assembled around the annulus (Paduano *et al.*, 1993; Day, 1993; Gysling and Greitzer, 1994; Weigl *et al.*, 1997), or operability enhancement, which implies alteration of the criticality of the bifurcation and elimination of the hysteresis associated with rotating stall (Eveker *et al.*, 1995, 1998; Liaw and Abed, 1996; Yeung and Murray, 1997; D'Andrea, *et al.*, 1998). With active control and the same stall margin, the compressor may operate stably near the peak of the compressor characteristic, resulting improvement of both operating range and performance. Experimentally there are essentially three basic types of actuation techniques that have been used in active control of rotating stall, namely inlet guide vanes (IGVs) (Paduano *et al.*, 1993), air injectors (Day, 1993; Gysling and Greitzer, 1994; D'Andrea *et al.*, 1998; Weigl *et al.*, 1998) and outlet bleed valves (Badmus *et al.*, 1993; Eveker *et al.*, 1995, 1998; Yeung and Murray, 1997). Freeman *et al.* (1998) used sleeve valves to recirculate air over the engine for active stall control, which is essentially a combination of bleed valves and injectors.

On the theoretical end, the design and analysis of controllers for rotating stall and surge control are based on the model developed by Moore and Greitzer in their seminal papers (Moore and Greitzer, 1986; Greitzer and Moore, 1986). The model is a set of nonlinear partial differential equations (PDEs) for pressure rise, averaged and disturbed values of flow coefficient as functions of time and circumferential position around the compressor. The Moore-Greitzer model captures most of the dynamic behavior of stall and surge and is sufficient for design and analysis of active controllers (Paduano *et al.*, 1993; Mansoux *et al.*, 1994; Gysling and Greitzer, 1994; Leonessa, *et al.*, 1997). The three state Moore-Greitzer model

is the Galerkin projection of the PDEs to the zeroth (axisymmetric) and the first spatial harmonics. One of the attractive features of the three state Moore-Greitzer model is that it captures the qualitative dynamic behavior of both surge and rotating stall, and is simple enough for designing active controllers (McCaughan, 1990; Liaw and Abed, 1996; Wang and Krstić, 1997; Eveker *et al.*, 1995, 1998). In the three state Moore-Greitzer model, rotating stall is identified as a transcritical bifurcation from the steady axisymmetric flow to the first circumferential modal wave, while deep surge is identified as a Hopf bifurcation from the steady axisymmetric flow to unsteady limit cycle oscillations of flow and pressure.

One of the major considerations in practical implementation of active stall control is the complexity of sensing and actuation (Ralph, 1993; Bansal, 1993). Since the rotating stall modes are rotating around the annulus of the compressor, distributed actuators are required to achieve controllability (Paduano *et al.*, 1993; Gysling and Greitzer, 1994; Weigl *et al.*, 1998). In Weigl *et al.*, 1998, 12 air injectors are used to stabilize the first and second harmonic. As the number of actuators is reduced, the rotating stall modes may become linearly uncontrollable (D'Andrea *et al.*, 1998). In D'Andrea *et al.*, three pulsed air injectors are used to eliminate the hysteresis, but the stall modes are unstabilizable. For bleed valve actuators located downstream, the effects of actuation is essentially axisymmetric (non axisymmetric effects decay exponentially in the axial direction), and the rotating stall modes are linearly uncontrollable (Eveker *et al.*, 1995, 1998). In order to reduce the complexity of the actuators, bifurcation control of rotating stall is one of the main design tools (Liaw and Abed, 1996).

The issue of magnitude and rate saturations becomes predominant in the practical implementation of active controllers on aeroengines. The growth time of the stall cell can be very short, usually several rotor revolutions. For instance, the time for stall cell formation is about 30 millisecond (3 rotor revolutions) at the stall inception point for a low speed compressor at Caltech (D'Andrea *et al.*, 1998), and the active stall control is unsuccessful using a bleed valve with bandwidth of 140 Hz (Yeung and Murray, 1997). The fast growth of stall precursors is due to the strong nonlinear effects in stall inception (Greitzer and Moore, 1986; Wang and Murray, 1998). The magnitude saturation for the actuator is unavoidable since in practice it is undesirable to bleed more than a small percentage of the flow through the core compressor in an aircraft engine. Also, the exogenous inputs, modeled as initial conditions to the model, cannot be treated as infinitely small due to the finite amplitude inlet swirl and distortions.

Although many controllers have been designed for bleed valve actuators using Lyapunov stability theory and dynamical system theory, too many to mention here, few have addressed the performance and effectiveness of the controllers. In Hendricks and Gysling (1994), gain and phase margins of different controllers based on the linearized Moore-Greitzer model are used to evaluate the effectiveness of different actuations. In Wang and Krstić (1997), effects of bandwidth were analyzed for a class of backstepping controllers. To the authors' knowledge, no work has done to simultaneously address the following issues in active stall control in a systematic way: the noise level, the actuator magnitude saturation, bandwidth and rate limits, and the shape of the compressor characteristic which is the major nonlinearity in the system. The goal of the current paper is to make sure these issues are understood based on theoretical analysis of the three state Moore-Greitzer model, numerical simulations of a high

fidelity model, and experiments on a low speed axial compressor.

The theoretical analysis on the three state Moore-Greitzer model allows us to get approximate analytical solution of the operability enhancement as a function of noise level, actuator magnitude and rate limits, and the shape of the compressor characteristic. We first reduce the order of the model by approximating the dynamics on the saddle-sink connections, which are the invariant manifold that captures the main dynamics of stall inception. Then we propose the *analysis problem* and the *synthesis problem* for the reduced system:

- **Analysis Problem** Given a control law with magnitude saturation and rate limits, how much operability enhancement can be achieved?
- **Synthesis Problem** Given a bleed valve actuator with magnitude saturation and rate limits, what is the optimal control law that gives the largest operability enhancement?

We prove that the synthesis problem is essentially a minimax problem. For the analysis problem, the qualitative effects of actuator limits and fluid noise on the operability enhancement are obtained by analyzing the reduced system using the approach of phase plane analysis. For the synthesis problem, we prove that for the reduced two dimensional system, the optimal control law is the bang on control that opens the bleed valve against its rate limit as soon as the sensors detect the stall cell has grown out of the noise level. For the optimal control, we derive analytic formulas for the operability enhancement as a function of the actuator magnitude and rate limits, the noise level, and the shape of the compressor characteristic. Experiments are also carried out on a low-speed single-stage rig using different levels of steady continuous air injections in the inlet duct to create a family of compressor characteristics. Simulations are done for a high fidelity model with 37 states. The results from the analytic formulas give good qualitative agreement with the experimental data and the simulations.

The paper is organized as follows. In Section 2 we provide the background information and the motivation from bifurcation theoretic point of view. In Section 3 we reduce the full four dimensional system to a two dimensional system, and we analyze the bifurcations and qualitative dynamics on the phase plane. Control analysis problem is set up and discussed. In Section 4, we define and solve the synthesis problem for the reduced two dimensional system and derive analytic formulas for the operability enhancement. Effects of time delay are also analyzed. In Section 5, we describe the high fidelity model, experiment setup, and experimental procedure. We compare the results from theoretical formulas, simulations of a high fidelity model, and experiments. Section 6 is the summary and conclusion.

2 Background and Motivation

In this section we describe the Moore-Greitzer model and the dynamics and bifurcations associated with rotating stall and surge. Then we discuss the benefit of bifurcation control. Finally, we motivate the effects of actuator limits from bifurcation theoretic point of view.

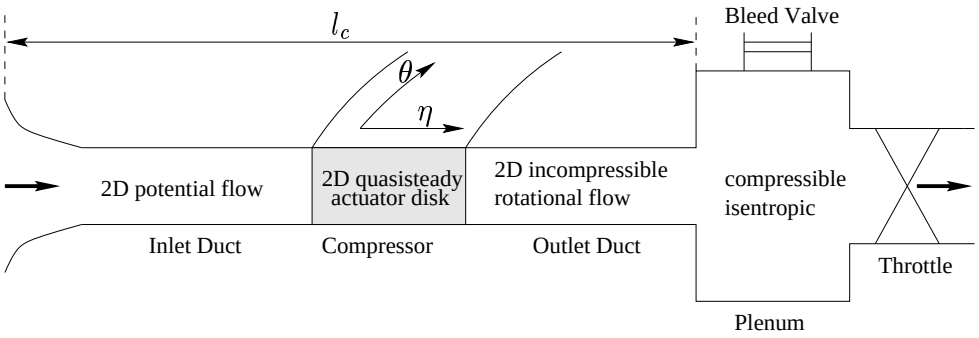

Figure 1: The composition of an axial compression system and assumptions on the flow

2.1 Background

The Moore-Greitzer model for an axial compression system

An axial compression system is composed of an inlet duct, a compressor, an outlet duct, a plenum, and a throttle (see Figure 1). The important assumptions of the Moore-Greitzer model are shown in Figure 1 (Moore and Greitzer, 1986). Also shown in the figure is the bleed valve actuator on the plenum. The flow in the inlet duct is assumed to be two dimensional potential flow, where η is in the axial direction and θ is in the circumferential direction. The compressor is modeled as two dimensional quasi-steady actuator disc, which implies that the pressure-rise across the compressor is given by

$$\frac{\Delta P}{\frac{1}{2}\rho U^2} = F(\varphi) - \tau \frac{d\varphi}{dt},$$

where U is the wheel speed at mean diameter, $\varphi = \varphi(\theta, \xi)$ is the local, unsteady axial velocity coefficient at the compressor face, $F(\varphi)$ is the axisymmetric steady performance of the blade row, τ is the coefficient of the pressure-rise lag. The flow in the outlet duct is modeled as linearized steady two dimensional rotational flow. The flow in the plenum is modeled as compressible, isentropic, and quiescent. Using these assumptions, Moore and Greitzer (1986) derived a set of partial differential equations (PDEs) for which the unknowns are the flow coefficient $\varphi(\theta, \xi)$ evaluated as the compressor face and the annulus-averaged pressure-rise coefficient $\Psi(\xi)$ across the compressor. By projecting the PDEs onto the zeroth and the first spatial harmonic, Moore and Greitzer (1986) derived a three-state model given by

$$\begin{aligned}
\frac{d\Phi}{d\xi} &= \frac{1}{l_c}\left(\frac{1}{2\pi}\int_0^{2\pi} \psi_c(\Phi + A\sin\zeta)\, d\zeta - \Psi\right), \\
\frac{d\Psi}{d\xi} &= \frac{1}{4B^2 l_c}\left(\Phi - \Phi_T(\Psi)\right), \\
\frac{dA}{d\xi} &= \frac{1}{\pi}\frac{1}{m+\mu}\int_0^{2\pi} \psi_c(\Phi + A\sin\zeta)\sin\zeta\, d\zeta,
\end{aligned} \tag{1}$$

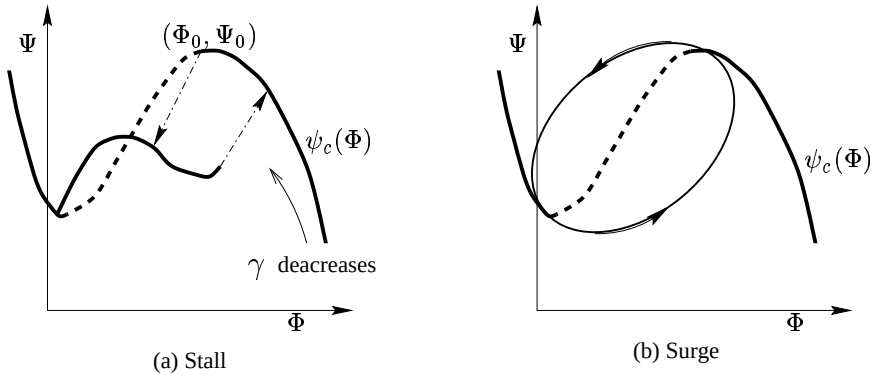

Figure 2: Stall and surge

where $\Phi(\xi) := \int_0^{2\pi} \varphi(\theta, \xi) d\theta$ is the annulus-averaged flow coefficient, A is the amplitude of the first harmonic of the axial flow disturbances around the compressor annulus, $\psi_c(\cdot)$ is the compressor characteristic, $\Phi_T(\cdot)$ is the throttle characteristic, l_c is the effective length of the compression system, B is the Greitzer B-parameter, m is the duct parameter, μ is the inertia parameter, ξ is the nondimensional time in rotor radians, ζ is the circumferential angle around the compressor annulus. Suppose the compressor characteristic is analytic and the throttle characteristic is $\Phi_T(\Psi) = (\gamma + u)\sqrt{\Psi}$, where u is the control input of the bleed valve and γ is the throttle coefficient denoting the opening of the throttle ($\gamma = 0$ means the throttle is fully closed). γ and B are the bifurcation parameters of the model (McCaughan, 1990). γ determines the operating condition, and rotating stall occurs when the throttle characteristic intersects the peak of the compressor characteristic. B is proportional to the size of the plenum and determines the axisymmetric dynamics Φ and Ψ. When B is large, the eigenvalues of the axisymmetric dynamics tends to become unstable near the peak of the compressor characteristic.

Properties of the dynamics of the model

We first discuss the dynamics and bifurcations for the uncontrolled system, i.e. $u = 0$. We treat the throttle coefficient γ as the bifurcation parameter. The shape of a typical compressor characteristic is shown in Figure 2.

The obvious equilibria of the system are the axisymmetric equilibria given by

$$\Phi = \Phi_e(\gamma), \quad \Psi = \Psi_e(\gamma) = \psi_c(\Phi_e(\gamma)), \quad J = 0.$$

where $J = A^2$. The axisymmetric equilibria denote the axisymmetric flow condition. There are two types of bifurcations of the axisymmetric equilibria.

- At the peak of the compressor characteristic $\gamma = \gamma_0$, a transcritical bifurcation to rotating stall occurs. The rotating stall equilibria denote the unsteady nonaxisymmetric flow which is a first modal traveling wave rotating around the annulus of the compressor at a fraction of the rotor speed.

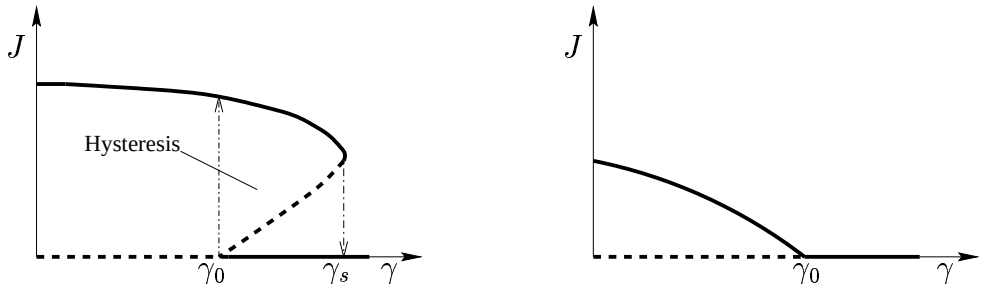

(a) Subcritical bifurcation

(b) Supercritical bifurcation

Figure 3: Subcritical and supercritical bifurcations.

- If B is large, then at a positive slope of the characteristic $\gamma = \gamma_{sg} < \gamma_0$, a Hopf bifurcation to surge occurs. The surge limit cycle denotes the axial unsteady axisymmetric flow and pressure oscillation across the compression system.

A complete numerical bifurcation analysis is in McCaughan (1990). Throughout this paper we assume B is small such that there is no Hopf bifurcation to surge. The transcritical bifurcation to rotating stall is typically subcritical, and there is a saddle-node bifurcation on the stalled branch (see Figure 3(a)). The stall inception is catastrophic because of the hysteresis associated with the subcritical bifurcation. It is easy to show that the stall mode A is linearly uncontrollable with bleed valve actuators. So it is impossible to design a state feedback to stabilize the axisymmetric equilibria beyond the peak of the compressor characteristic. Nevertheless, Liaw and Abed (1996) designed a feedback control law $u = KJ$ such that the bifurcation of the closed loop system is supercritical. By changing the criticality of the bifurcation, the stall inception becomes progressive and more benign (see Figure 3(b)).

2.2 Motivation from bifurcation theoretic point of view

Due to actuator magnitude and rate saturation, the actual domains of attraction of the stable operating points could be small. In this section we motivate the effects of actuator saturation limits from bifurcation theoretic point of view.

Consider the a feedback control law with magnitude and rate saturation constraint and first order dynamics

$$\dot{u} = \chi(\Phi, \Psi, J; u_{mag}, u_{rate}, \tau), \tag{2}$$

where u_{mag} and u_{rate} are magnitude and rate saturation limits, i.e.,

$$0 \le u \le u_{mag}, \quad -u_{rate} \le \dot{u} \le u_{rate},$$

and τ is the time constant associated with the actuator. Especially, we consider the feedback control law $u = KJ$ with first order actuator dynamics constrained by magnitude and rate

saturations given by

$$
\begin{aligned}
\frac{d\Phi}{d\xi} &= \frac{1}{l_c}\left(\frac{1}{2\pi}\int_0^{2\pi}\psi_c(\Phi + A\sin\zeta)\,d\zeta - \Psi\right),\\
\frac{d\Psi}{d\xi} &= \frac{1}{4B^2 l_c}\left(\Phi - (\gamma+u)\sqrt{\Psi}\right),\\
\frac{dA}{d\xi} &= \frac{1}{\pi}\frac{1}{m+\mu}\int_0^{2\pi}\psi_c(\Phi + A\sin\zeta)\sin\zeta\,d\zeta,\\
\frac{du}{d\xi} &= \begin{cases} -u_{rate} & \text{if } \dfrac{u_{des}-u}{\tau} \le -u_{rate},\\[2ex] \dfrac{u_{des}-u}{\tau} & \text{if } \left|\dfrac{u_{des}-u}{\tau}\right| < u_{rate},\\[2ex] u_{rate} & \text{if } \dfrac{u_{des}-u}{\tau} \ge u_{rate}, \end{cases}\\
u_{des} &= \begin{cases} 0 & \text{if } KJ \le 0,\\ KJ & \text{if } 0 < KJ < u_{mag},\\ u_{mag} & \text{if } KJ \ge u_{mag}, \end{cases}
\end{aligned}
\tag{3}
$$

together with the magnitude constraint $0 \le u \le u_{mag}$.

The effects of actuator limits (magnitude saturation, bandwidth and rate limits) and fluid noise on rotating stall control can be motivated from the bifurcation analysis point of view. A typical bifurcation diagram for the uncontrolled three state Moore-Greitzer model is in Figure 4(a). The region of attraction of the stable axisymmetric equilibrium is the shaded region in Figure 4(a). Now consider the controller with infinite magnitude saturation limit and infinite bandwidth, i.e., the bleed valve can bleed out as much air as we want and is infinitely fast, then the bifurcation diagram for the closed loop system is shown in Figure 4(b). The bifurcation for the stall equilibria is supercritical and the stall inception is progressive. The stall branch can be arbitrarily close to the axisymmetric equilibrium by increasing K. The region stabilized by control is shown in Figure 4(b).

Now suppose the magnitude saturation for the actuator is finite but the actuator bandwidth is infinite, i.e., the valve is infinitely fast but it can only bleed out a certain amount of air. The bifurcation diagram for the closed loop system is shown in Figure 4(c). The thick solid and dash lines denote the equilibria for the closed loop system. It can be seen from this figure that there is a new saddle-node like bifurcation point S_K due to the actuator magnitude saturation. This saddle-node like bifurcation point defines γ_K such that any arbitrarily small noise of J will drive the system to the fully developed rotating stall equilibrium if the throttle operates at a position such that $\gamma < \gamma_K$. Also we have

$$\lim_{K\to+\infty}\gamma_K = \gamma_0^* = \gamma_0 - u_{mag},$$

where γ_0^* is the throttle coefficient of the stall inception point when the bleed valve is fully open. It is clear from Figure 4(c) that the bleed valve controller cannot eliminate the hysteresis

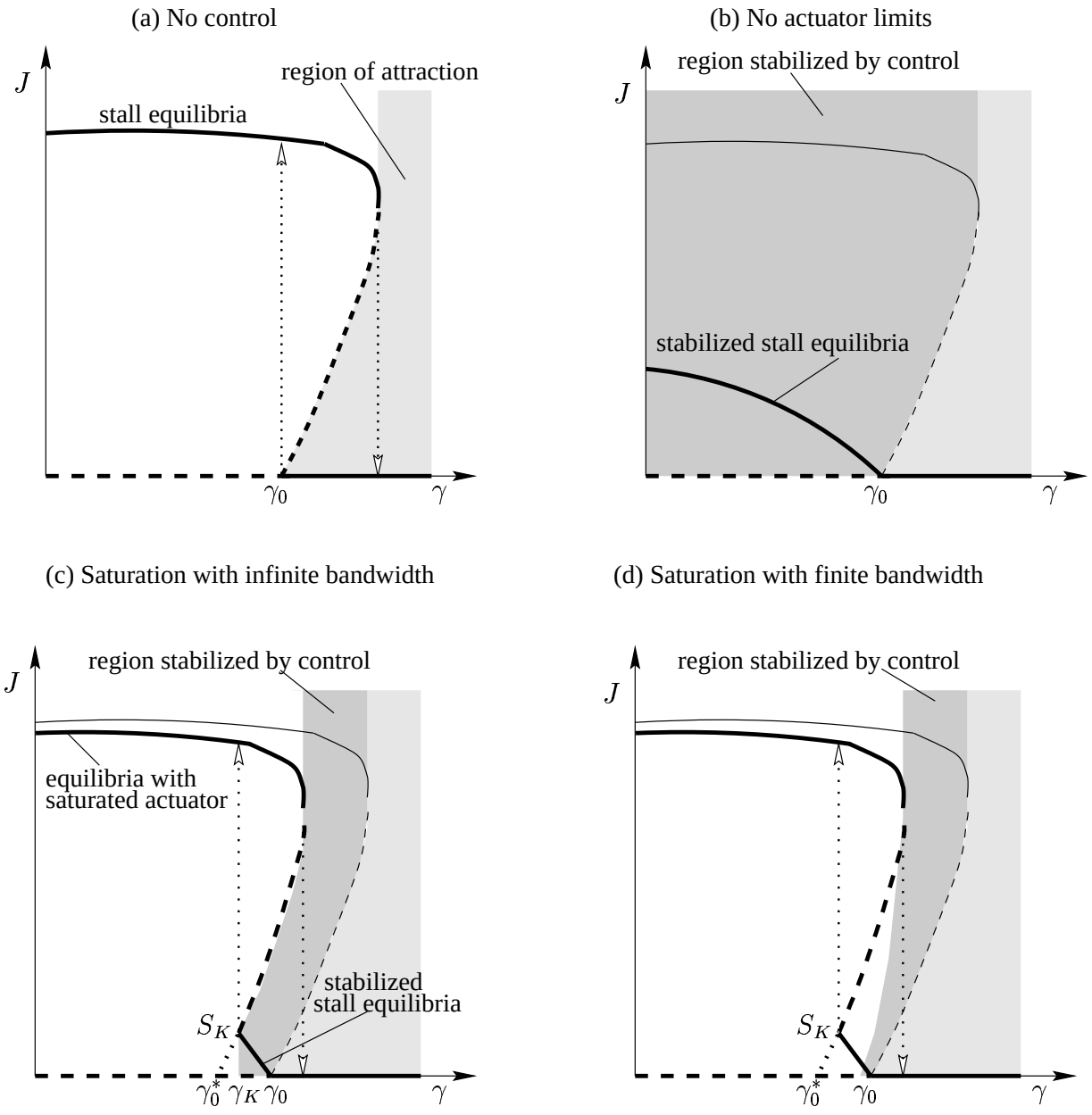

Figure 4: Bifurcation diagrams for the effects of actuator limits.

loop if its magnitude saturation is finite. Furthermore, any arbitrary small noise of J will grow to fully developed rotating stall no matter how large the controller gain is when the throttle operates at a position such that $\gamma < \gamma_0^*$. It can also be seen that the region stabilized by control is much smaller than the previous case if u_{mag} is small. This implies it is impossible to build a valve with small air bleed to achieve a large extension of operable range.

Now, in addition to the finite magnitude saturation assumption, suppose the bandwidth and rate limits are finite, i.e., the bleed valve opens and closes with a finite speed. Also assume the bleed valve is initially closed, i.e., $u(0) = 0$. Then the region stabilized by control is shown in Figure 4(d). By comparing (c) and (d), it is clear that the region of attraction from control is further restrained by the actuator bandwidth and rate limits. It can be proved in later sections that if the rate limits goes to zero, then the region of attraction from control becomes arbitrarily small.

The noise level for a real compression system is not arbitrarily small due to disturbances such as inlet distortion and inlet turbulence level. We model the noise as a closed set of initial conditions of J. When the noise level is of finite amplitude, the open loop system goes to rotating stall at a throttle coefficient larger than the nominal stall inception point γ_0. The extension of operable range becomes even smaller if the noise level is of finite amplitude.

It should be noted that in the above discussions are valid only if the initial conditions for Φ and Ψ are close to the axisymmetric equilibrium for a fixed throttle coefficient and B is small enough such that there no surge dynamics. In the following sections we will systematically develop the ideas in the above discussions and obtain analytical estimates for the controller performance in the presence of noise, actuator magnitude saturation and rate limits.

3 Control Analysis

In this section we reduce the four dimensional system (3) into a two dimensional system. We give qualitative phase portraits for the reduced system for different throttle settings. It turns out that the stable manifold of a saddle equilibrium in the system is the boundary between two regions: one with the trajectories converging to the stabilized stall equilibrium, the other with the trajectories converging to the fully developed stall equilibrium.

3.1 System reduction and approximation

Numerical bifurcation analysis by McCaughan (1990) confirmed the typical qualitative phase portraits of the open loop system for different γ's look like Figure 5 if the Greitzer B-parameter is small enough. Let Φ_0, Ψ_0 and γ_0 be the axial flow coefficient, the pressure rise coefficient, and throttle coefficient at the peak of the compressor characteristic, respectively. Let γ_s be the throttle coefficient at which the unstable stall equilibria merge with the stable stall equilibria. It is clear that the saddle-sink connections in Figure 5 are attracting (stable) and they captures the instabilities (rotating stall) of the Moore-Greitzer model. The main effort of this section is to approximate the dynamics on the saddle-sink connection.

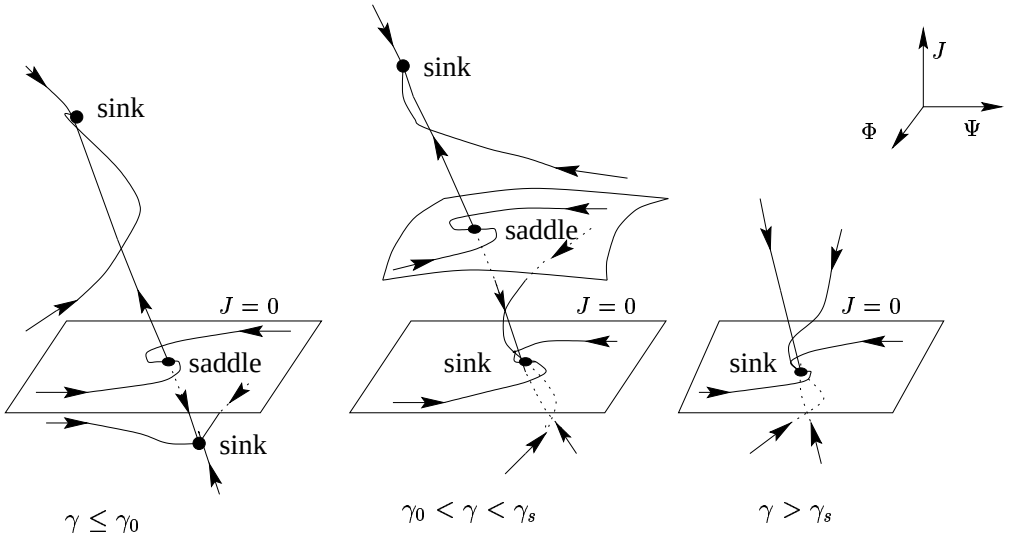

Figure 5: Phase portraits for the three state Moore-Greitzer model at different throttle coefficients.

The following proposition gives the center manifold reduction of the controlled system. We use the convention $\mathcal{O}(x^n)$ to represent terms of the order $\|x\|^n$ and higher, where $x \in \mathbb{R}^n$.

Proposition 3.1 *For sufficiently small B, the dynamics of (3) near the transcritical bifurcation point $(\Phi_0, \Psi_0, 0)$ can be approximated by the dynamics on the center manifold and can be approximated by the following two dimensional system*

$$\frac{dJ}{d\xi} = \alpha_1(\delta + u)J + \alpha_2 J^2 + \mathcal{O}\left(J[\delta\ u\ J]^2\right), \tag{4}$$

$$\frac{du}{d\xi} = \begin{cases} -u_{rate} & \text{if } \dfrac{u_{des} - u}{\tau} \leq -u_{rate}, \\ \dfrac{u_{des} - u}{\tau} & \text{if } \left|\dfrac{u_{des} - u}{\tau}\right| < u_{rate}, \\ u_{rate} & \text{if } \dfrac{u_{des} - u}{\tau} \geq u_{rate}, \end{cases} \tag{5}$$

$$u_{des} = \begin{cases} 0 & \text{if } KJ \leq 0, \\ KJ & \text{if } 0 < KJ < u_{mag}, \\ u_{mag} & \text{if } KJ \geq u_{mag}, \end{cases}$$

where $J = A^2$, $\delta = \gamma - \gamma_0$,

$$\alpha_1 = \frac{2\sqrt{\Psi_0}\psi_c''}{m+\mu}, \tag{6}$$

$$\alpha_2 = \frac{1}{4(m+\mu)}\left(\psi_c''' + \frac{\gamma_0 \psi_c''^2}{\sqrt{\Psi_0}}\right), \tag{7}$$

and all the derivatives of ψ_c *are evaluated at* Φ_0.

The proof of Proposition 3.1 is the standard center manifold reduction (Guckenheimer and Holmes, 1983), and is given in Appendix A. Here are several observations from Proposition 3.1.

(1) Suppose $u = 0$, the coefficients α_1 and α_2 in the center manifold equation determine the bifurcation characteristics of the uncontrolled Moore-Greitzer model in the neighborhood of γ_0.

(2) For a typical compressor characteristic we have $\psi_c'' < 0$, so $\alpha_1 < 0$. α_1 is the sensitivity of the eigenvalue of the stall mode to variations of the bifurcation parameter γ. It is easy to see that if $|\psi_c''|$ and Ψ_0 are large, which is typical of the high speed compressor of an aircraft engine, then $|\alpha_1|$ is large and the system quickly goes linearly unstable beyond the bifurcation point.

(3) If $\alpha_2 > 0$, then the transcritical bifurcation to rotating stall is subcritical; if $\alpha_2 < 0$, then the transcritical bifurcation to rotating stall is supercritical. The subcritical bifurcation is typical of axial compression systems and is more detrimental in that there is a hysteresis and the stall inception is catastrophic. The positivity of α_2 implies nonlinear instability which accelerates the growth rate of rotating stall once it is out of the linearly dominated region. Also, the positivity of α_2 is the main reason why active control of rotating stall requires high bandwidth actuators. This point will become more clear in the later sections. α_2 increases quadratically with ψ_c'', and increases linearly with ψ_c'''. If the unstable (left) part of the characteristic becomes steeper, then $\psi_c''' >$ and α_2 become larger, and the nonlinear instability becomes more severe. Later in the experiment section the unstable part of the characteristic is leveled by upstream steady air injections and the rate requirement of bleed valve actuator is drastically reduced.

(4) The minimum gain for feedback control law $u = KJ$ to make the closed loop system be supercritical is $K^* = -\frac{\alpha_2}{\alpha_1}$. It is clear that K^* increases as $|\psi_c''|$ and ψ_c''' increase. This is also true for the rate requirement and will be shown in later sections.

Since the equation (4) only captures the local behavior near the bifurcation point, we use the following system to approximate the dynamics on the attracting saddle-sink connections to capture the hysteresis behavior (see Figure 5):

$$\dot{J} = \alpha J\left(\alpha_1(\delta + u) + \sum_{k=2}^{n} \alpha_k J^{k-1}\right), \tag{8}$$

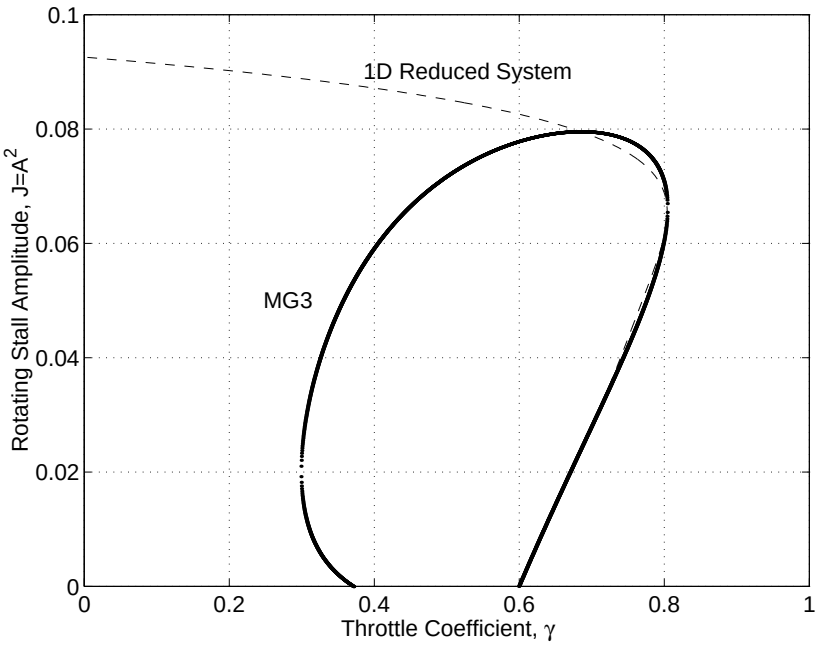

Figure 6: The stall equilibria of the MG3 and the approximate 1D system for the Caltech rig.

where u is the control input given by (5), and the α's are selected such that the equilibria of the ordinary differential equation (8) fit the rotating stall equilibria in γ-J plane in the following way:

1) α_1 and α_2 are taken from the center manifold equation (6) and (7).

2) α_k $(k = 3, \cdots, n)$ are selected such that the equilibria of the one dimensional system (8) fit the equilibria of the full system in the hysteresis region.

3) α is selected such that the growth rate of J for the approximate system (8) matches that for the full system at $\gamma = \gamma_0$.

This choice is designed to give an approximation that matches the local bifurcation characteristics while simultaneously matching the magnitude and growth rate of fully developed rotating stall. Figure 6 show the stall equilibria for the three state Moore-Greitzer model for the Caltech rig with a fourth order polynomial compressor characteristic and the stall equilibria for the reduced system with $n = 7$.

Throughout this paper we make the following assumptions on the shape of the stall equilibrium branch:

(A1) The bifurcation of the open loop system is subcritical, i.e., $\alpha_2 > 0$.

(A2) There is only one saddle-node bifurcation on the stall equilibrium branch. The bifurcation point is at $\delta_s := \gamma_s - \gamma_0$.

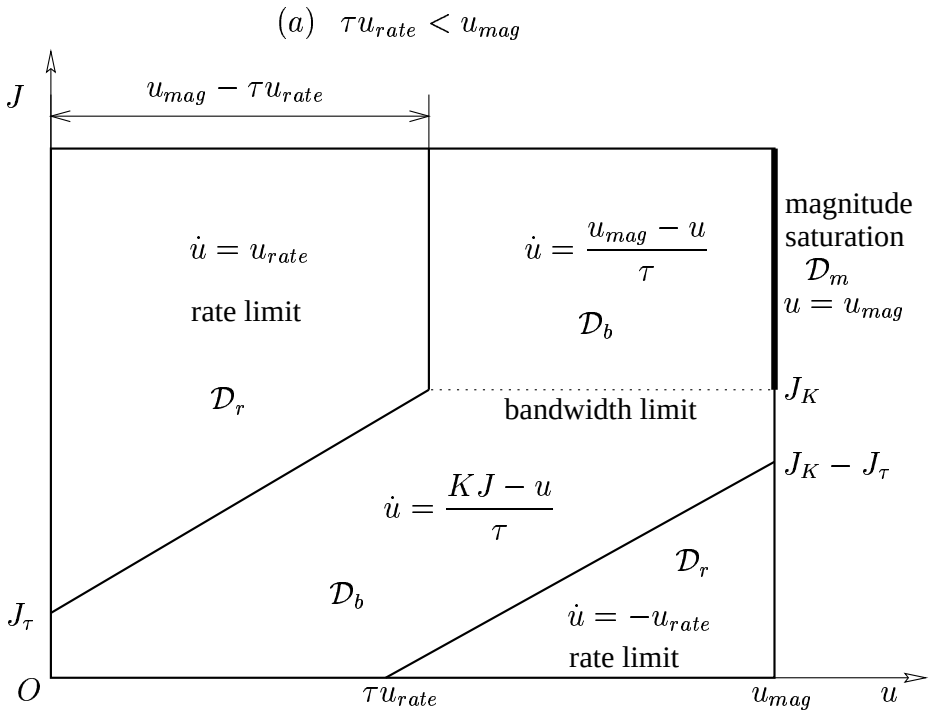

Figure 7: Control laws in u-J plane when $\tau u_{rate} < u_{mag}$.

We remark here that assumption (A2) may not be true for δ's for the full model (see Figure 6), but it is true in a neighborhood of $\delta = 0$, which is sufficient for our analysis since the magnitude saturation limit u_{mag} is small, and the Moore-Greitzer model is not an accurate model when the throttle operates far away to the left of the peak of the characteristic.

3.2 Bifurcations and phase portraits of the reduced system

In the following we describe the qualitative dynamics of the reduced two dimensional system (5) and (8) by providing the phase portraits for different throttle coefficients.

Due to the magnitude saturation and the rate limits, different regions in the u-J phase plane are governed by different control laws. Let

$$J_K = \frac{u_{mag}}{K}, \quad J_\tau = \frac{\tau u_{rate}}{K},$$

Then we have the following two cases. If $\tau u_{rate} < u_{mag}$, then there are three regions in the phase space: the bandwidth limited region $\mathcal{D}_b$, the rate limited region $\mathcal{D}_r$, and the magnitude saturation part $\mathcal{D}_m = \{(u, J) | \, u = u_{mag}, J > J_K\}$ (see Figure 7). If $\tau u_{rate} > u_{mag}$, then there are two regions: the bandwidth limited region $\mathcal{D}_b$, and the magnitude saturation part $\mathcal{D}_m$ (see Figure 8). Due to the magnitude saturation constraint, the phase space is only limited to the region $0 \leq u \leq u_{mag}$, and $J \geq 0$.

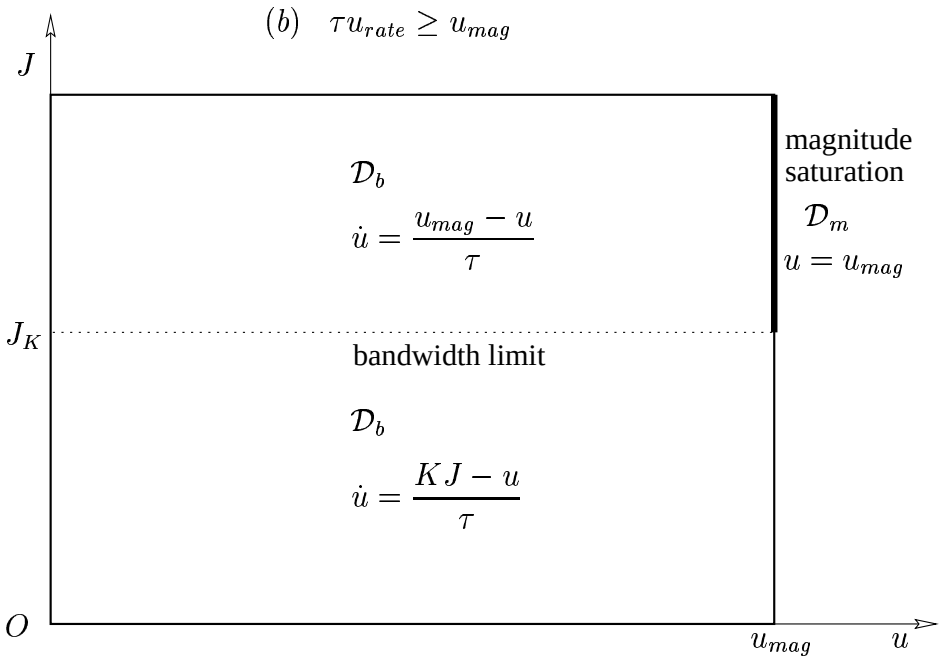

Figure 8: Control laws in u-J plane when $\tau u_{rate} \geq u_{mag}$.

Let

$$\gamma_s^* = \gamma_s - u_{mag}, \quad \gamma_H \approx \gamma_0 - \frac{\alpha_1 K + \alpha_2}{\alpha \alpha_1 \alpha_2 \tau}, \quad \gamma_K = \gamma_0 - u_{mag} - \frac{1}{\alpha_1} h\left(\tfrac{u_{mag}}{K}\right), \quad \tau_H \approx \frac{K}{\alpha \alpha_2 u_{mag}},$$

where $h(J) := \sum_{k=2}^{n} \alpha_k J^{k-1}$. Assuming $u_{mag} < \gamma_s - \gamma_0$, the qualitative phase portraits for the reduced two dimensional system (8) and (5) at different operating throttle positions are shown in Figure 9. The sequence of the figures is when the throttle is closing beginning from the stable side of the compressor characteristic, i.e., when the throttle coefficient γ is decreasing.

(1) Figure 9(a) shows that if the throttle is operated at a throttle position γ such that $\gamma > \gamma_s^*$, then the axisymmetric equilibria O is the only equilibrium and it is globally stable.

(2) Figure 9(b) shows that if the throttle is operated at γ such that $\gamma = \gamma_s^*$, then saddle-node bifurcation occurs. The equilibrium splits into two as γ decreases.

(3) Figure 9(c) shows that if the throttle is operated at γ such that $\gamma_0 < \gamma < \gamma_s^*$, then two equilibria are born from the saddle node bifurcation. S_1 is a saddle denoting the unstable stall equilibrium when the actuator is fully open. S_2 is a sink denoting the stable stall equilibrium when the actuator is fully open. There are two different regions in the u-J plane divided by the stable manifold of the saddle S_1, denoted by $W^s(S_1)$:

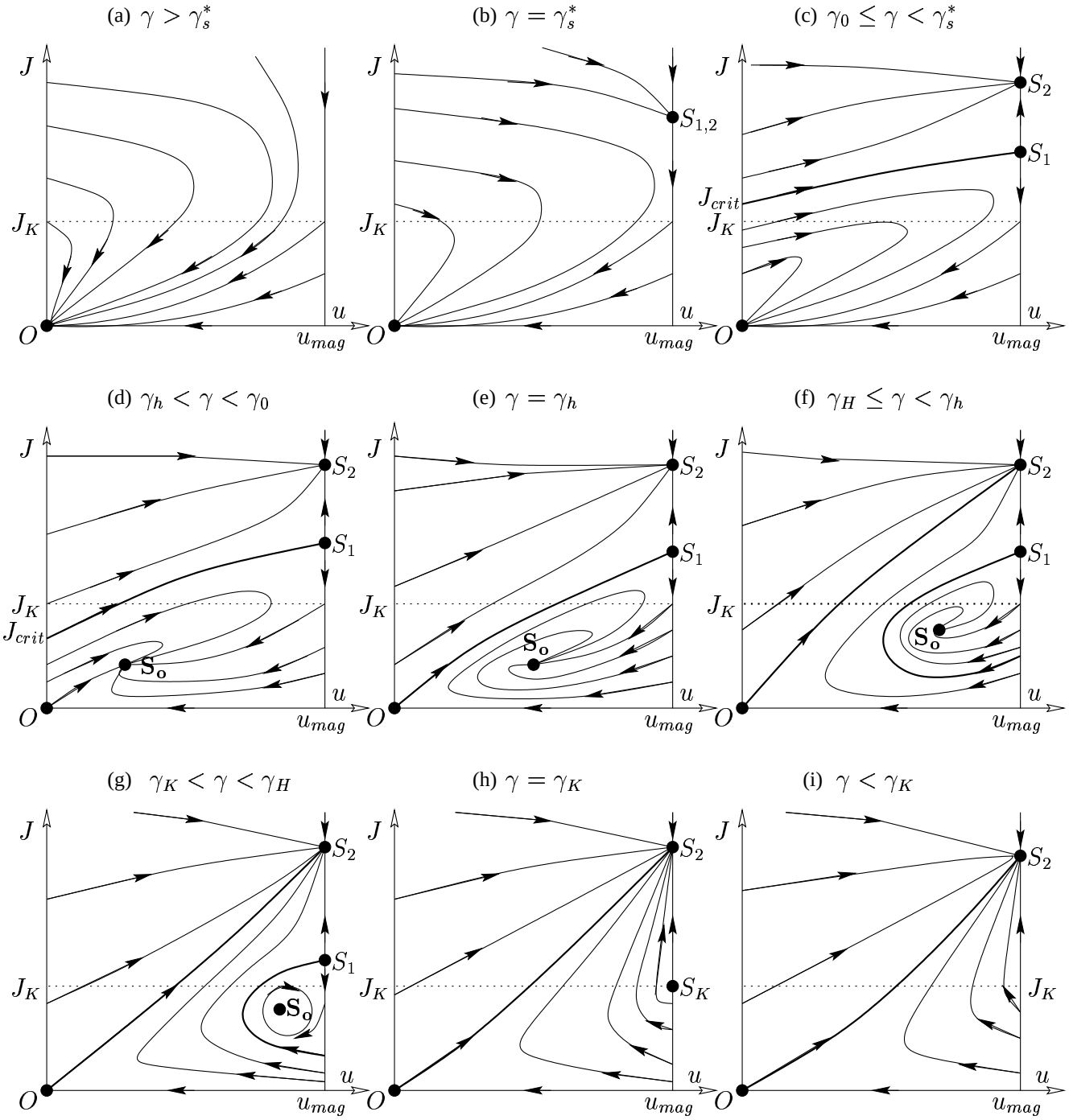

Figure 9: Qualitative phase portraits of the reduced system.

the trajectories above $W^s(S_1)$ converge to the fully developed rotating stall equilibrium S_2, while the trajectories below $W^s(S_1)$ converge to the stable axisymmetric equilibrium O.

(4) Figure 9(c) shows at $\gamma = \gamma_0$, i.e., the throttle is operated at the peak of the compressor characteristic, a transcritical bifurcation occurs on the axisymmetric equilibrium O.

(5) Figure 9(d) shows that if the throttle is operated at γ such that $\gamma_h < \gamma < \gamma_0$, then the stabilized stall equilibrium S_o is born from the axisymmetric equilibrium O. At the same time, O becomes a saddle. The trajectories below $W^s(S_1)$ converge to the stabilized stall equilibrium S_o.

(6) Figure 9(e) shows that when $\gamma = \gamma_h$, heteroclinic connection occurs between the unstable axisymmetric equilibrium O and the unstable stall equilibrium S_1, and the heteroclinic orbit is structurally unstable. This implies that if the bleed valve actuator is initially closed, i.e., $u(0) = 0$, then any nonzero initial condition of J would go to fully developed rotating stall and at the same time the actuator saturates. γ_h can be found numerically by integrating a point near S_1 backward in time at different throttle coefficients.

(7) Figure 9(f) shows that if the throttle is operated at γ such that $\gamma_H < \gamma \leq \gamma_h$, then the heteroclinic connection is broken and $W^s(S_1)$ is connecting $u = u_{mag}$ instead of $u = 0$. An interesting point is that if the initial condition of J is small, then for any initial condition of u, the trajectory will go to the fully developed stall equilibrium S_2; while if the initial condition of J is not too small, then there exist initial conditions of u such that the trajectory goes to the stabilized stall equilibrium S_o.

(8) Suppose $\tau > \tau_H$, then at $\gamma = \gamma_H$, a Hopf bifurcation occurs on the stabilized stall branch S_o: S_o becomes unstable and stable limit cycles are born (see Figure 9(g)). If $\tau \leq \tau_H$, then there is no Hopf bifurcation on the stabilized stall branch S_o. Here we assume $\gamma_h > \gamma_H$.

(9) Figure 9(h) shows that at $\gamma = \gamma_K$, the source S_o, the stable limit cycle, and the saddle S_1 are all collapsed together through a degenerate saddle-node bifurcation.

(10) Figure 9(i) shows that if the throttle is operated at γ such that $\gamma < \gamma_K$, then the degenerate node S_K disappears and every trajectory except $u = 0$ converges to the fully developed stall equilibrium S_2.

If $u_{mag} > \gamma_s - \gamma_0$, then we have $\gamma_s^* < \gamma_0$. This implies the saddle-node bifurcation of the stalled branch is at a lower throttle coefficient than that of the peak of the compressor characteristic.

A typical phase portrait for the reduced system for the case (d) in Figure 9 is given by Figure 10. The main new feature of the phase portrait is that there is strongly attracting manifold whose physical meaning is that the fully developed stall occurs and the bleed valve opens until it saturates.

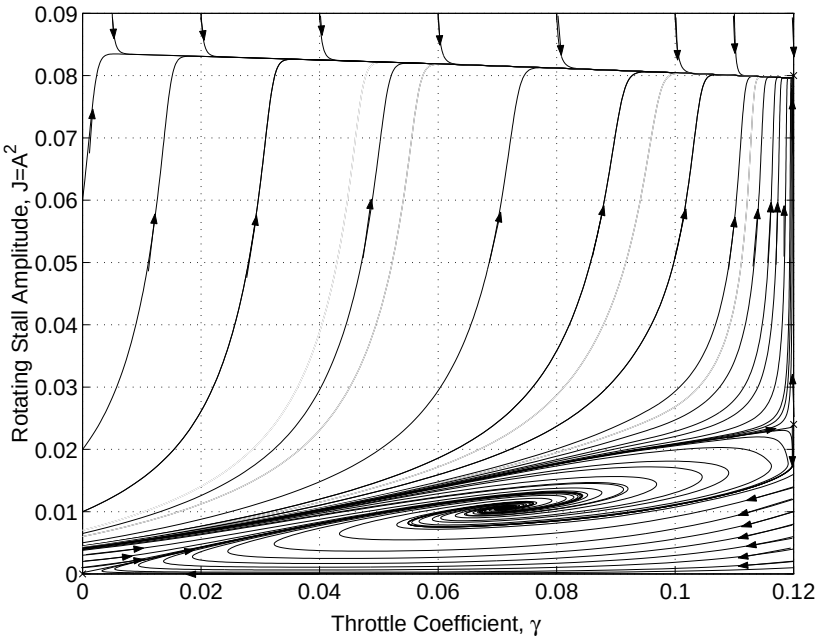

Figure 10: A typical phase portrait for the reduced system for the case (d) in Figure 9. The main throttle is operated at 4 percent of the stall flow to the left of the peak. The values of the parameters are: $u_{mag} = 0.12$, $u_{rate} = 0.0385$, $\tau = 0.6293$, $\delta = -0.036$, $K = 2K^* = 6.7257$. Here $K^* := -\frac{\alpha_2}{\alpha_1}$ is the minimum gain such that the bifurcation for the closed loop system is supercritical. The equilibria are denoted by "x".

3.3 Control analysis

In this section we give the problem statement of control analysis. We omit the solution here for the control law (5), but we sketch the ideas of how to solve the problem. In the next section we given a solution to the "bang-on" control, which is a limiting case of the control law (5).

The noise in the flow through the compressor is a complicated issue. The turbulence level in the inlet flow may be the source of localized disturbances. But other disturbances such as inlet swirl and inlet distortion may have larger amplitude. In this paper we model the noise as a closed set of initial conditions for J in the system, i.e.,

$$\mathcal{E} = \{J \mid 0 \leq J \leq \epsilon\},$$

where ϵ is the largest initial condition for J and is called the noise level. We remark here that in practice ϵ can be increasing as the throttle coefficient γ decreases. In this paper we assume ϵ is a constant.

The operability boundary $\delta(\mathcal{E}, u)$ for the reduced system (8) and (5) is defined as the minimum throttle coefficient δ at which none of the trajectories with initial conditions $u(0) = 0$

and $J(0) \in \mathcal{E}$ reaches the fully developed rotating stall equilibrium. The operability enhancement is defined as the difference between the stability of the uncontrolled system and that of the controlled system, i.e.,

$$\Delta(\mathcal{E}, u) := \delta(\mathcal{E}, 0) - \delta(\mathcal{E}, u).$$

The control analysis problem is: given all the parameters in the control law (5) and determine the operability enhancement $\Delta(\mathcal{E}, u)$.

It is trivial to show that the operability boundary for the uncontrolled system is given by $\delta(\mathcal{E}, 0) = -\frac{1}{\alpha_1}\sum_{k=2}^{n} \alpha_k \epsilon^{k-1} \approx -\frac{\alpha_2 \epsilon}{\alpha_1} > 0$. This implies that rotating stall occurs to the right of the peak of the characteristic. Now from Figure 9 it is clear that at the operability boundary of the controlled system, we have $J_{crit} = \epsilon$, where J_{crit} is the y-coordinate of the intersection between $W^s(S_1)$, the stable manifold of S_1, and the straight line $u = 0$. J_{crit} can be determined by integrating backward in time of the local stable manifold of S_1. Exact analytic solution of $W^s(S_1)$ can be difficult to find since the system is nonlinear and $W^s(S_1)$ might travel through different regions with different control laws (see Figure 7 and 8). But we can obtain approximate solution of $W^s(S_1)$ assuming the shape and matching the boundary conditions at $u = 0$ and $u = u_{mag}$. We omit the details here, but we will illustrate the idea in the next section for the bang-on control law. The stable manifold $W^s(S_1)$ can also be found by numerical integration of the reduced system with an initial condition near the saddle S_1 backward in time. The stability boundary can be found by binary search on γ until $J_{crit} = \epsilon$ is satisfied.

4 Control Synthesis

In this section we claim the "bang-on" control law is optimal in the sense that it maximizes the operability enhancement when there are magnitude and rate limits on the actuators. We derive approximate formulas for the operability enhancement as a function of noise and actuator limits. The formulas will be used in the next section to compare with experiments and simulations to a high fidelity model.

4.1 System reduction and bang-on control law

In the following we consider the control input u in the function set $\mathcal{U}$ defined as

$$\mathcal{U} := \{u \mid 0 \le u \le u_{mag}, |\dot{u}| \le u_{rate}, u \text{ is piecewise smooth}\}.$$

The goal is to find the control laws to maximize the operability enhancement. As for the control analysis problem, we first reduce the order of the Moore-Greitzer model with control $u(\xi) \in \mathcal{U}$.

Proposition 4.1 *If B is small, $\psi_c(\cdot)$ is analytic, and the axisymmetric disturbances are small, then the Moore-Greitzer model (1) with control input $u \in \mathcal{U}$ can be approximated by*

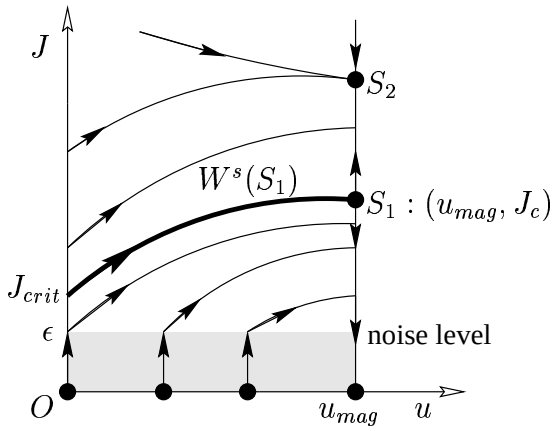

Figure 11: Phase portrait for bang-on control.

the following one dimensional system:

$$\dot{J} \;=\; \alpha J \left(\alpha_1(\delta + u) + \sum_{k=2}^{n} \alpha_k J^{k-1} \right), \tag{9}$$

where δ_1 and α_2 are given by (6) and (7), respectively, and other α's are selected in the same way as in Section 3.1.

The reduction is the similar to Proposition 3.1 and is given in the Appendix A.

The "bang-on" controller is defined as

$$\dot{u} = \begin{cases} 0 & \text{if } J \le J_{thresh}, \text{ or } J > J_{thresh} \text{ and } u = u_{mag}, \\ u_{rate} & \text{if } J > J_{thresh} \text{ and } 0 \le u < u_{mag}, \end{cases} \tag{10}$$

where ξ is the nondimensional time, and J_{thresh} is the threshold. Usually J_{thresh} is set to be above the noise level, i.e., $J_{thresh} > \epsilon$. The "bang-on" control law can be obtained from the control law (5) by increasing K and decreasing τ. Then the bandwidth limit region $\mathcal{D}_b$ shrinks to empty and the whole phase region is rate limited. A phase portrait for the reduced system (9) with the bang on control law is given by Figure 11. It should be mentioned that the line segment $\{(u, J) \mid 0 \le u \le u_{mag}, J = 0\}$ forms a continuum of equilibria, with $(u_{mag}, 0)$ being stable and all others being unstable. It should be mentioned that for the bang-on control law (10) the actuator is not actuated if the stall disturbance is in the noise level. If the actuator is actuated when the disturbances are under the noise level, induced oscillations might occur. Consider the following control law:

$$\dot{u} = \begin{cases} -u_{rate} & \text{if } J \le J_{thresh}, \\ 0 & \text{if } J > J_{thresh} \text{ and } u = u_{mag}, \\ u_{rate} & \text{if } J > J_{thresh} \text{ and } 0 \le u < u_{mag}. \end{cases} \tag{11}$$

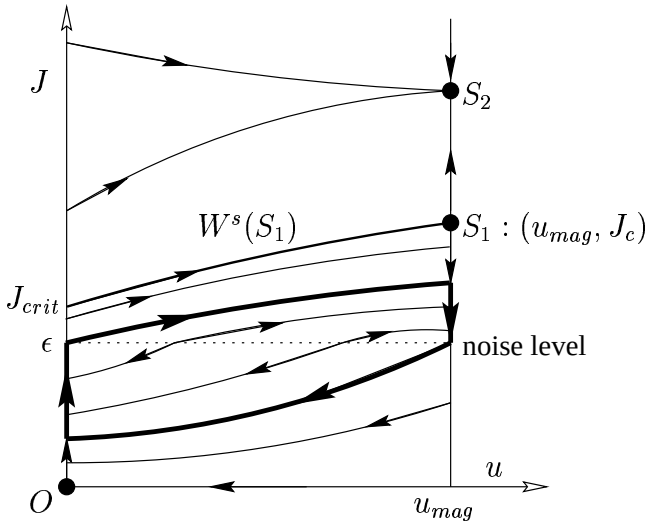

Figure 12: A phase portrait for bang-on control.

The actuator would close if the disturbance is under the noise level. A phase portrait for the reduced system (9) with control law (11) is shown in Figure 12. It can be seen that a stable limit cycle exists, and the actuator experiences magnitude and rate saturations during the cycle. In practice, this would lead to "chattering" of the actuator, and the system may become unstable if there are sensing uncertainties and delays.

4.2 Problem formulation

Let $\mathcal{A}_\delta = \{J \mid 0 \leq J \leq a(\delta)\}$, $a(\delta)$ denotes the maximum amount of rotating stall that can be tolerated. Usually $a(\delta)$ is chosen to be larger than the noise level and smaller than the magnitude of fully developed stall. The noise set is given by $\mathcal{E} = \{J \mid 0 \leq J \leq \epsilon\}$. In the following we assume $a(\delta) = J_c(\delta)$, where $J_c(\delta)$ is the y-coordinate of the saddle S_1 (see Figure 11). Let $u(0)$ be an initial condition for u. We assume $u(0) = 0$, which means that the bleed valve is initially closed. Let $(J_\delta(\xi; e), u_\delta(\xi; e))$ be the trajectory of (9) from the initial condition $(J(0), u(0)) = (e, 0)$. We say the initial condition e is $\mathcal{A}_\delta$ attractive if $\limsup_{\xi\to\infty} J_\delta(\xi; e) \leq a(\delta)$. We define the operability boundary for the initial condition e and the control $u(\xi)$ as $\delta_c(u, e) := \min\{\delta \mid e \text{ is } \mathcal{A}_\delta\text{-attractive}\}$. Define $\delta_c(u, \mathcal{E}) := \max_{e\in\mathcal{E}} \delta_c(u, e)$ as the operability boundary for the noise level $\mathcal{E}$ with control $u(\xi)$, and $\delta_o(\mathcal{E}) := \delta_c(0, \mathcal{E})$ as operability boundary for the uncontrolled system. In other words, $\delta_c(u, \mathcal{E})$ is the minimum throttle coefficient such that non of the trajectories for (9) and control $u(\xi)$ with initial conditions $u(0) = 0$ and $J(0) \in \mathcal{E}$ goes to the fully developed rotating stall. We define the operability enhancement as $\Delta(u, \mathcal{E}) := \delta_c(0, \mathcal{E}) - \delta_c(u, \mathcal{E})$. The optimal control problem is a minimax problem defined as finding a control $u^* \in \mathcal{U}$, such that the operability enhancement

is maximized, i.e.,

$$\begin{aligned}\Delta(u^*, \mathcal{E}) &= \max_{u\in\mathcal{U}} \Delta(u, \mathcal{E}) \\ &= \delta_o(\mathcal{E}) - \min_{u\in\mathcal{U}} \max_{e\in\mathcal{E}} \delta_c(u, e).\end{aligned}$$

Theorem 4.1 *Suppose the assumptions (A1) and (A2) are true. Let* $\mathcal{A}_\delta = \{J \mid 0 \le J \le J_c(\delta)\}$, *where* $J_c(\delta)$ *is the y-coordinate of the saddle* S_1 *(see Figure 11). Then for any* $e \in \mathcal{E}$, *we have*

$$\begin{aligned}\delta_c(u^*, e) &= \min_{u\in\mathcal{U}} \delta_c(u, e), \\ \delta_c(u^*, e^*) &= \min_{u\in\mathcal{U}} \max_{e\in\mathcal{E}} \delta_c(u, e),\end{aligned}$$

where $e^* = \epsilon$, *and*

$$u^* = \begin{cases} u_{rate}\xi & \text{if } 0 \le \xi < \xi_2, \text{ and } J > \epsilon, \\ u_{mag} & \text{if } \xi \ge \xi_2, \text{ and } J > \epsilon, \end{cases} \tag{12}$$

and $\xi_2 := \frac{u_{mag}}{u_{rate}}$.

A sketch of the proof of Theorem 4.1 is based on the simple fact that for the system (9) and (12), the stable manifold of the saddle S_1, denoted as $W^s(S_1)$, is monotonously increasing as u increases from 0 to u_{mag}. Also, any trajectory for the system (9) with a controller $u \in \mathcal{U}$ cannot intersect $W^s(S_1)$ transversally from above. A sketch of the proof is given in Appendix B. The types of control laws for the disturbances in the noise level do not affect the operability enhancement. To avoid the chattering effects, we set $\dot{u} = 0$ for $J \le \epsilon$.

4.3 Calculation of operability enhancement

Now we consider the reduced order system with the optimal control u^* and the worst noise e^*. The goal is to solve for $W^s(S_1)$. Specifically, we consider the following system

$$\dot{J} = \alpha_1(\delta + u)J + \alpha_2 J^2, \tag{13}$$

$$\dot{u} = \begin{cases} 0 & \text{if } J \le \epsilon, \text{ or } J > \epsilon \text{ and } u = u_{mag}, \\ u_{rate} & \text{if } J > \epsilon \text{ and } 0 \le u < u_{mag}, \end{cases} \tag{14}$$

with initial conditions and final conditions

$$\begin{aligned} u(0) = 0, &\quad u(\xi_2) = u_{mag}, \\ J(0) = \epsilon, &\quad J(\xi_2) = -\tfrac{\alpha_1}{\alpha_2}(u_{mag} + \delta), \end{aligned} \tag{15}$$

Let

$$\Delta^* = 1 + \frac{\alpha_1\delta}{\alpha_2\epsilon}, \quad \eta = \alpha_2\epsilon\xi, \quad f = \frac{J}{\epsilon}, \quad \lambda = \frac{\sigma}{\eta_2},$$

$$\sigma = \frac{-\alpha_1 u_{mag}}{\alpha_2\epsilon}, \quad \eta_2 = \alpha_2\epsilon\xi_2, \quad f' = \frac{df}{d\eta}, \quad J(\xi_2) = \epsilon(\sigma + 1 - \Delta^*).$$

Then the equations (13) and (14) with initial and final conditions (15) can be written as follows.

$$\begin{aligned} f' &= (\Delta^* - 1 - \lambda\eta)f + f^2, && (16)\\ f(0) &= 1, && (17)\\ f(\eta_2) &= 1 + \sigma - \Delta^*. && (18) \end{aligned}$$

The exact solution of (16) with initial condition (17) and final condition (18) is given by the following integral-algebraic equation

$$1 - \frac{e^{-\left(\frac{\sigma}{2}+1-\Delta^*\right)\eta_2}}{1+\sigma-\Delta^*} = \int_0^1 \eta_2 e^{-\left(\frac{\sigma}{2}\zeta^2+(1-\Delta^*)\zeta\right)\eta_2} d\zeta. \qquad (19)$$

Suppose the solution to (19) is $\Delta^*(\sigma, \eta_2)$, it is easy to see that if $\eta_2 = 0$, then $\Delta^*(\sigma, \eta_2) = \sigma$. This implies that the operability enhancement is σ if the bleed valve actuator is infinitely fast. The following proposition gives the operability enhancement when the bleed valve is slow.

Proposition 4.2 *If $\eta_2 \gg \sigma$, then $\Delta^*(\sigma, \eta_2) = \dfrac{\sigma}{\eta_2} + \mathcal{O}\left(\dfrac{\sigma^2}{\eta_2^2}\right)$.*

To prove the proposition, we need the following lemma on asymptotic properties of the incomplete Γ-function.

Lemma 4.1 *Define the incomplete Γ-function as*

$$\Gamma(\alpha, x) = \int_x^\infty e^{-t} t^{\alpha-1} dt, \quad (\alpha > 0)$$

then as $x \to \infty$, $\Gamma(\alpha, x)$ can be expressed as the following series

$$\Gamma(\alpha, x) = x^{\alpha-1} e^{-x} \left[\sum_{m=0}^{M-1} \frac{(-1)^m \Gamma(1-\alpha+m)}{x^m \Gamma(1-\alpha)} + \mathcal{O}\left(x^{-M}\right) \right],$$

where the Γ-function $\Gamma(\alpha)$ is defined as

$$\Gamma(\alpha) = \int_0^\infty e^{-t} t^{\alpha-1} dt.$$

Proof of Proposition 4.2: Define the *complementary error function* as

$$\operatorname{erfc}(x) = \frac{2}{\sqrt{\pi}} \int_x^\infty e^{-t^2} dt = 1 - \frac{2}{\sqrt{\pi}} \int_0^x e^{-t^2} dt.$$

It is trivial to show

$$\operatorname{erfc}(x) = \frac{1}{\sqrt{\pi}} \Gamma\left(\frac{1}{2}, x^2\right).$$

By Lemma 4.1, we know for $x \approx \infty$,

$$\operatorname{erfc}(x) = \frac{1}{\sqrt{\pi}} e^{-x^2} \left(\frac{1}{x} - \frac{1}{2x^3} \right) + \mathcal{O}\left(\frac{e^{-x^2}}{x^5} \right). \tag{20}$$

Consider the integral in the right hand side of the integral-algebraic equation (19), it can be show by straightforward calculation that

$$\begin{aligned} RHS &= \int_0^1 \eta_2 e^{-\left(\frac{\sigma}{2}\zeta^2 + (1-\Delta)\zeta\right)\eta_2} d\zeta \\ &= \sqrt{\frac{\pi\eta_2}{2\sigma}} e^{\frac{(1-\Delta)^2}{2\sigma}\eta_2} \left[\operatorname{erfc}\left(\sqrt{\frac{\eta_2}{2\sigma}}(1-\Delta) \right) - \operatorname{erfc}\left(\sqrt{\frac{\eta_2}{2\sigma}}(1-\Delta+\sigma) \right) \right] \\ &= \frac{1}{1-\Delta} - \frac{\sigma}{\eta_2(1-\Delta)^3} - \frac{e^{-\left(\frac{\sigma}{2}+1-\Delta\right)\eta_2}}{1+\sigma-\Delta} + \mathcal{O}\left(\frac{1}{{\eta_2}^3} \right). \end{aligned}$$

We have utilized (20) in the last equality. Now by equating this to the left hand side of (19), we get

$$\Delta(1-\Delta)^2 = \frac{\sigma}{\eta_2} + \mathcal{O}\left(\frac{1}{{\eta_2}^3} \right). \tag{21}$$

Suppose $\Delta^*(\sigma, \eta_2)$ be the solution to this equation. Let $\eta_2 \to \infty$, we have $\Delta^*(\sigma, \eta_2) \to 0$ or $\Delta^*(\sigma, \eta_2) \to 1$.

Now we show that

$$\lim_{\eta_2 \to \infty} \Delta^*(\sigma, \eta_2) \neq 1.$$

By substituting $\Delta^*(\sigma, \eta_2) = 1$ into the integral-algebraic equation (19), we get

$$LHS = 1 - \frac{1}{\sigma} e^{-\frac{1}{2}\sigma\eta_2},$$

$$RHS = \sqrt{\frac{2\eta_2}{\sigma}} \int_0^{\sqrt{\frac{\sigma\eta_2}{2}}} e^{-\zeta^2} d\zeta = \sqrt{\frac{\pi\eta_2}{2\sigma}} + \mathcal{O}(1), \qquad (\eta_2 \approx \infty).$$

Hence, when $\eta_2 \approx \infty$, $LHS \neq RHS$. So we have

$$\lim_{\eta_2 \to \infty} \Delta^*(\sigma, \eta_2) = 0.$$

By solving (21), we get

$$\Delta^*(\sigma, \eta_2) = \frac{\sigma}{\eta_2} + \mathcal{O}\left(\frac{1}{{\eta_2}^2} \right).$$

■

The implication of Proposition 4.1 is that when $\eta_2 \gg \sigma$, i.e., the bleed valve is very slow, the noise is large, or the compressor characteristic is very steep near the peak, then the operability enhancement is given by

$$\Delta(u^*, \mathcal{E}) = \frac{\alpha_2 \epsilon}{-\alpha_1} \Delta^* \approx \frac{4(m+\mu) u_{rate}}{\epsilon \left(\psi_c''' + \frac{\gamma_0 \psi_c''^2}{\sqrt{\Psi_0}} \right)}. \tag{22}$$

This implies that the operability enhancement decreases if either the noise level ϵ, or $|\psi_c''(\Phi_0)|$, or $\psi_c'''(\Phi_0)$ increases. If the rate limit u_{rate} decreases, then the operability enhancement decreases. In the multi-stage high speed compressor in air craft engines, $|\psi_c''(\Phi_0)|$ increases sharply as the engine speed increases, so the operability enhancement is expected to reduce drastically when engine speeds up. The third derivative ψ_c''' denotes the relative curvature on each side of the peak. If the left (unstable) side is steeper (or shallower) than the right (stable) side, then $\psi_c''' > 0$ (or $\psi_c''' < 0$), then formula (22) implies that the operability enhancement decreases as the unstable part of the compressor characteristic becomes steeper. This result is interesting because the effectiveness of the controller is determine by the unseen (unstable part of the characteristic cannot be directly measured in experiments). The experiment in the next section proves this point, i.e., the rate requirement for the actuator reduced drastically when the unstable part of the characteristic is made shallower by steady air injection upstream of the rotor.

It might be difficult to solve $\Delta^*(\sigma, \eta_2)$ explicitly from (19). In the following we solve $\Delta^*(\sigma, \eta_2)$ by approximating the stable manifold of the saddle. Suppose $W^s(S_1)$ is the stable manifold of the saddle S_1 in the (η, f) plane, and $W^s(S_1)$ is parameterized by $f = f(\eta)$ in the (η, f) plane. Then from (16), (17) and (18) we get the boundary conditions of $W^s(S_1)$

$$\begin{array}{ll} f(0) = 1, & f(\eta_2) = 1 + \sigma - \Delta^*, \\ f'(0) = \Delta^*, & f'(\eta_2) = 0. \end{array} \tag{23}$$

We assume $f(\eta)$ has the following form

$$\begin{aligned} f(\eta) &= \bar{f} \left(1 - C \frac{2\sigma}{\pi(1+\sigma)} g(\eta) \right), \\ g(\eta) &= \arctan \left(\frac{\pi\lambda}{4\sigma} (1+\sigma)(\eta - \eta_2)^2 \right), \end{aligned} \tag{24}$$

where the unknowns $\bar{f}$ and C are to be determined by boundary conditions. Letting $f(\eta)$ satisfy the boundary conditions (23), and considering that $\sigma \gg 1$ in practice, we get

$$\Delta_1^*(\sigma, \eta_2) = \frac{\sigma}{1 + \frac{1}{8}\pi\sigma{\eta_2}^2 \arctan\left(\frac{1}{4}\pi\sigma\eta_2\right)}. \tag{25}$$

If we use the form of (24) to satisfy the following boundary conditions of $W^s(S_1)$

$$\begin{array}{ll} f(0) = 1, & f(\eta_2) = 1 + \sigma - \Delta^*, \\ f'(\eta_2) = 0, & f''(\eta_2) = -\lambda(1 + \sigma - \Delta^*), \end{array} \tag{26}$$

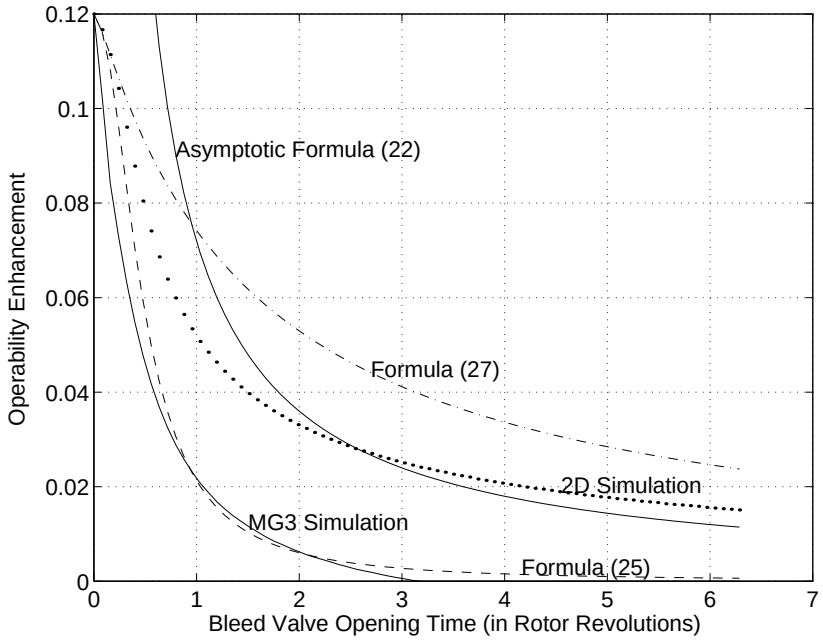

Figure 13: Comparison of operability enhancement for the bang-on control law obtained through simulations of the full Moore-Greitzer model and the reduced 2D model, and the predictions of the formulas (25), (27) and the asymptotic formula (22). The y-axis is the operability enhancement normalized by the throttle coefficient at the peak of the characteristic, γ_0.

then we get

$$\Delta_2^*(\sigma, \eta_2) = \sigma \frac{1 - \frac{2}{\pi} \arctan\left(\frac{\pi}{4}(1+\sigma)\eta_2\right)}{1 - \frac{2}{\pi}\frac{\sigma}{1+\sigma} \arctan\left(\frac{\pi}{4}(1+\sigma)\eta_2\right)}. \tag{27}$$

The comparisons for predictions of the formulas (22), (25), and (27), and numerical simulation of the full Moore-Greitzer model and the reduced two dimensional system is given by Figure 13. Although the formulas do not match the simulations qualitatively, they give the same trend as the bleed valve rate limit is reduced. The formulas (25) and (27) will be used in the next section to compare with the experimental results and the simulations of a high fidelity model for a low speed compressor.

4.4 Effects of time delay

In this section, we present the effects of time delay on the operability enhancement for the bang-on control. Finite bandwidths of sensors, the filters, and the computer hardware cause time delay between the actual flow signal at the sensor position and the control input in the control logic embedded in the compressor. Spatial separation between the downstream

bleed valve and the stall disturbances within the compressor is another source of time delay due to the compressibility and the inertia of air. The main point of this section is that the operability enhancement decreases *exponentially* with time delay, noise level, and the second and third derivatives of the compressor characteristic.

By considering the time delays, the bang-on control law is give by

$$\dot{u}^* = \begin{cases} 0 & \text{if } 0 \le \xi < \xi_1, \\ 0 & \text{if } \xi \ge \xi_1,\ J \le \epsilon; \text{ or } \xi \ge \xi_1\ J > \epsilon,\ u = u_{mag}, \\ u_{rate} & \text{if } \xi \ge \xi_1, \text{ and } J > \epsilon, \end{cases} \tag{28}$$

with initial condition $u(0) = 0$. Here ξ_1 is the time delay. Assuming $\xi_1 \ll \frac{u_{mag}}{u_{rate}}$ and u_{rate} is small, then by similar asymptotic analysis as in the rate limits case, the operability enhancement is given by

$$\Delta_d(u^*, \mathcal{E}) \approx \frac{\alpha_2 \epsilon}{-\alpha_1} \cdot \frac{\sigma}{\bar{\eta} e^{\eta_1}} = \Delta_r e^{-\frac{\epsilon \xi_1}{4(m+\mu)} \left(\psi_c''' + \frac{\gamma_0 \psi_c''^2}{\sqrt{\Psi_0}} \right)}, \tag{29}$$

where

$$\sigma = \frac{-\alpha_1 u_{mag}}{\alpha_2 \epsilon}, \quad \eta_1 = \alpha_2 \epsilon \xi_1, \quad \bar{\eta} = \frac{\alpha_2 \epsilon u_{mag}}{u_{rate}}, \quad \Delta_r = \frac{4(m+\mu) u_{rate}}{\epsilon \left(\psi_c''' + \frac{\gamma_0 \psi_c''^2}{\sqrt{\Psi_0}} \right)}.$$

Here Δ_r is the operability enhancement for the pure rate limit case. It can be seen that the time delay is more detrimental than rate limit since the operability enhancement decreases exponentially with the time delay ξ_1, the noise level ϵ, and the second and third derivatives of the compressor characteristic at the peak, while in the pure rate limit case, the operability enhancement depends on the reciprocal of these parameters. For high speed multi-stage compressors, the curvature of the compressor characteristic near the peak is large, so the operability enhancement could be very sensitive to time delays.

5 High Fidelity Simulations and Experiments

In this section we introduce a high fidelity model for simulations, and describe experiments to measure rate requirement for different compressor characteristics actuated by different level of steady air injection upstream. We compare the predictions of rate requirement from the theoretic formulas derived in the previous section, the simulation results and the experiments.

5.1 Simulation model

In this section we only give a sketch of the simulation model, more details can be found in Mansoux et al. (1994) and Yeung (1998). As mentioned in Section 2.1, the Moore-Greitzer PDE model is composed of a PDE for the local flow coefficient $\varphi(\theta, \xi)$ around the annulus of the compressor and an ODE for the annulus averaged pressure rise coefficient $\Psi(\xi)$. The model proposed by Mansoux et al. (1994) is a projection of the PDE to the $2N + 1$ equally

spaced points around the annulus of the compressor using discrete Fourier transform. In other words, the Mansoux model is the N mode representation of the PDE using $2N+1$ equally spaced points around the compressor annulus. So the Mansoux model is composed of $2N+1$ ODEs for the flow coefficient around the annulus and one ODE for pressure rise coefficient $\Psi(\xi)$, i.e., it has $2N+2$ states.

For the Mansoux model mentioned above, the damping for each mode is the same. But in reality, higher order modes tend to have more damping. This effect is accounted by the unsteady loss dynamics (Haynes *et al.*, 1994), which is modeled as a first order lag to the steady-state loss. The steady-state loss is the difference between the isentropic pressure rise and the actual pressure rise for stationary flow. The unsteady loss is the difference between the isentropic pressure rise and the actual pressure rise when the flow is unsteady. More specifically, the unsteady loss is modeled by the following first order ODEs:

$$\begin{aligned}
\Psi_c &= \Psi_{c,\text{isen}} - L_r - L_s, \\
\dot{L_r} &= \frac{1}{\tau_r}(L_{r,\text{ss}} - L_r), \\
L_{r,\text{ss}} &= R(\Psi_{c,\text{isen}} - \Psi_c), \\
\dot{L_s} &= \frac{1}{\tau_s}(L_{s,\text{ss}} - L_s), \\
L_{s,\text{ss}} &= (1-R)(\Psi_{c,\text{isen}} - \Psi_c),
\end{aligned}$$

where Ψ_c denotes the quasi-static compressor characteristic, $\Psi_{c,\text{isen}}$ the isentropic compressor characteristic, L_r the losses associated with the rotor, L_s the losses associated with the stator, R the reaction, and subscript ss steady-state. Now, for each of the $2N+1$ points around the compressor annulus, we have a rotor loss L_r and and a stator loss L_s. So there are $2N+1$ states for L_r and $2N+1$ states for L_s. So the total number of states for the uncontrolled Mansoux model is $6N+4$. We also need to model the dynamics of the actuator such as magnitude, bandwidth, and rate limitations. For the simulations reported in this paper, a simulation with five Fourier modes ($N=5$) resulting in 34 states for the compressor, and 3 states for the bleed actuator is used.

5.2 Experimental setup

The Caltech compressor rig is a single-stage, low-speed, axial compressor with sensing and actuation capabilities. Figure 14 shows a magnified view of the sensor and injection actuator ring and Figure 15 a drawing of the rig. The compressor is an Able Corporation model 29680 single-stage axial compressor with 14 blades, a tip radius of 8.5 cm, and a hub radius of 6 cm. Experiments are run with a rotor frequency of 100 Hz, giving a tip Mach number of 0.17. Rotating stall is observed under this condition in the rig with a frequency of 65 Hz. Data taken for a stall transition event suggest that the stall cell grows from the noise level to its fully developed size in approximately 30 msec (3 rotor revolutions).

Six static pressure transducers with 1000 Hz bandwidth are evenly distributed along the annulus of the compressor. A discrete Fourier transform is performed on the signals from

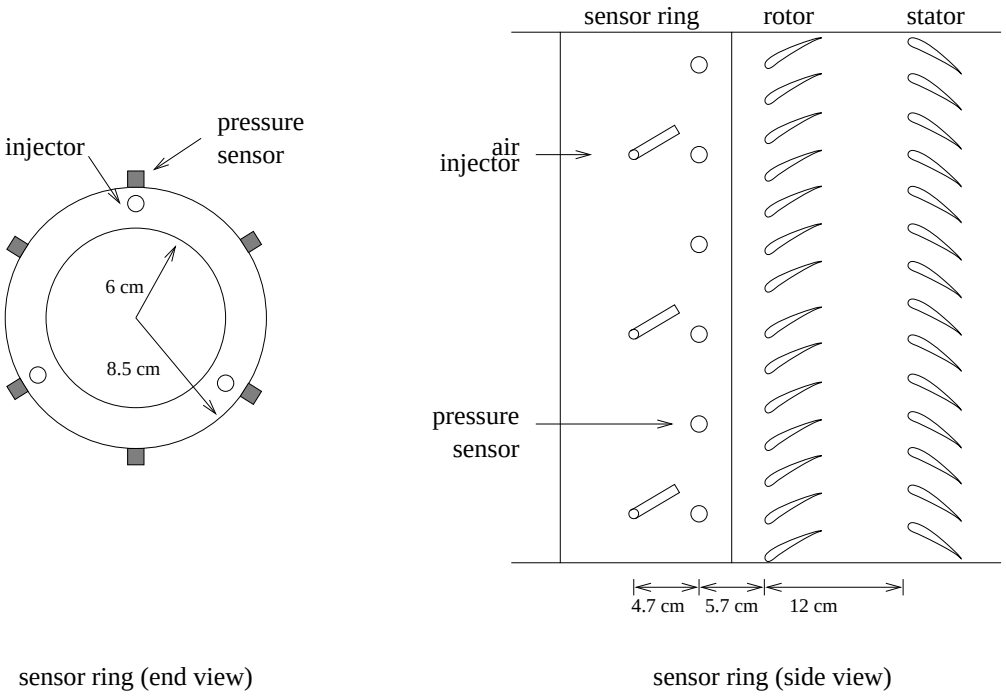

Figure 14: Sensor and injection actuator ring.

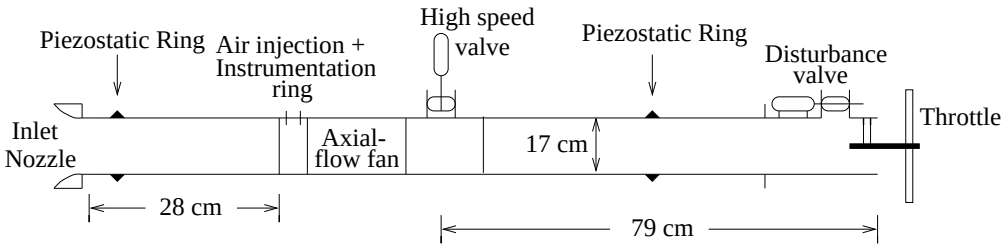

Figure 15: Experimental setup.

the transducers, and the amplitude and phase of the first and second mode of the stall cell associated with the total-to-static pressure perturbation are obtained. The difference between the pressure obtained from one static pressure transducer mounted at the piezostatic ring at the inlet and that from one mounted at another piezostatic ring downstream near the outlet of the system is computed as the pressure rise across the compressor. A high speed valve that is capable of bleeding 12% of the flow at the stall inception point is used for control of rotating stall. A low speed valve is used to move the operating points (change the throttle coefficient γ) of the system. Three air injectors are used to change the shape of the compressor characteristic $\psi_c(\cdot)$.

5.3 Experimental procedures

During the experiments, the injector angle relative to the axial flow direction is varied between 27° and 40° in the opposite direction of the rotor rotation, and the back pressure of the injectors is varied between 40 to 60 psi, producing a total of 16 different scenarios with air injection and one for the nominal open-loop system without air injection. At the various injection settings, experiments are carried out to obtain the rate values required for peak stabilization. For this study, peak stabilization is achieved if the conditions $\Phi \geq 0.9\Phi_0$ and $A \leq 0.5A_{\text{nom}}$ are met during the experiment, where Φ is the nondimensional axial velocity, A the amplitude of the first Fourier mode, Φ_0 the nondimensional axial velocity at stall inception, and A_{nom} the amplitude of fully developed stall without bleed valve control. It should be noted that Φ_0 and A_{nom} are different for each of the air injector settings. The experiment procedure is as follows. First set the throttle at the stable side of the characteristic to make sure there is no stall. By turning off the controller and closing the throttle, stall point of the open loop system is recorded. Then reset the throttle to the stable side of the characteristic, increase the rate and gain, and close the throttle to the open loop stall point. This procedure is repeated by increasing the rate until the conditions of peak stabilization are met. Among the 17 injection settings, peak stabilization is achieved in 11 cases and the nominally stable side of the compressor characteristic is experimentally recorded at each of the 11 settings. The unstable sides for each of these cases are identified by using surge cycles data with an algorithm proposed by Behnken (1996). For this study, a fourth order polynomial is used to approximate the piecewise continuous curve for each case. The polynomial compressor characteristics are to be used in simulations to the Mansoux model and the theoretical formulas (25) and (27) in the next section. The fitted compressor characteristics for three injector settings are shown in Figure 16.

5.4 Comparisons of theory, simulations, and experiments

Based on the functional dependence of the analytical relations for the minimum rate requirement on $\psi_c''(\Phi_0)$ and $\psi_c'''(\Phi_0)$, an examination of Figure 16 would indicate that expt5 should require the least rate while expt7 should require the most. The theory and simulations are expected to show at least a qualitative trend with respect to the experiment. With the back pressure to the air injectors being 55 psi, Figure 17 shows the open loop and closed loop

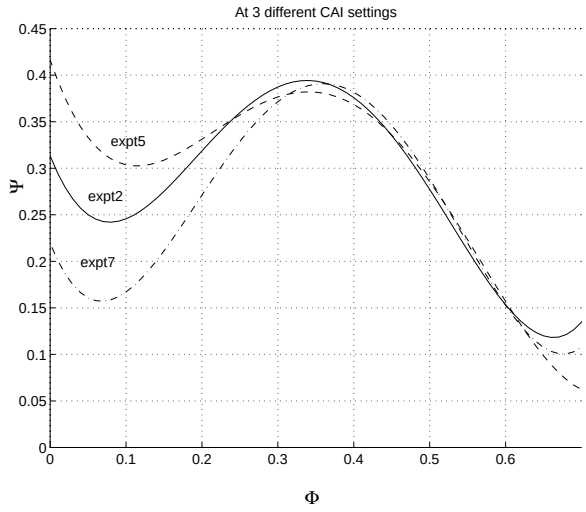

Figure 16: Identified compressor characteristics at 3 different continuous air injection settings.

behavior in the Φ-Ψ plane and the γ-J plane. The subcritical bifurcation of the open loop system associated with stall inception is changed to supercritical for the closed loop system. An interesting phenomenon is that the amplitude of the first stall mode becomes smaller when the throttle is operated around 0.37. This is because at these throttle values, the second mode dominates the compressor stall. Another interesting behavior of the closed loop system in the Φ-Ψ plane is that the stabilized stall branch tilts to the right of the peak before folding back to the left. The phenomenon is different from the closed loop system behavior in the experiments of Eveker *et al* (1995, 1998): the stabilized stall branch tilts to the left of the peak. The back-tracking stall branch can be explained from the three state Moore-Greitzer model as follows.

From the center manifold analysis in Appendix A, we know that for the control law $u = KJ$, the center manifold is given by

$$\phi = \sqrt{\Psi_0}\delta + \frac{\gamma_0 \psi_c''}{8\sqrt{\Psi_0}} J + \text{h.o.t.} \tag{30}$$

$$\psi = \frac{\psi_c''}{4} J + \text{h.o.t.} \tag{31}$$

where $\phi = \Phi - \Phi_0$, $\psi = \Psi - \Psi_0$. On the other hand, for the control law $u = KJ$, the dynamics on the center manifold is given by

$$\dot{J} = \alpha_1(\delta + KJ)J + \alpha_2 J^2 + \text{h.o.t.}$$

So on the stabilized stall branch, we have

$$\delta = -\left(K + \frac{\alpha_2}{\alpha_1}\right) J, \tag{32}$$

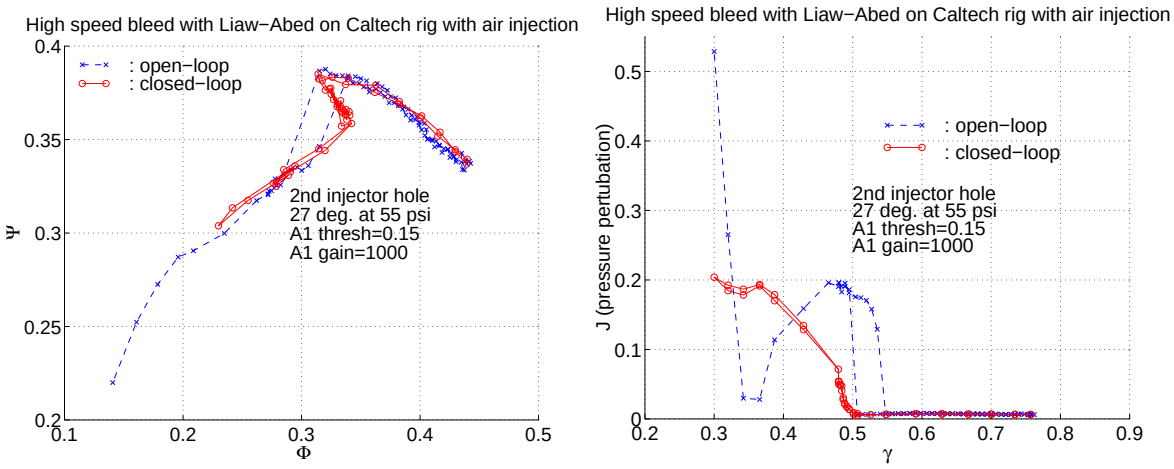

Figure 17: Open- and closed-loop behavior of system on Φ-Ψ plane for control with bleed valve and continuous air injection at 55 psi injector back pressure.

where α_1 and α_2 are given by (6) and (7), respectively. Now, by substituting (32) into (30) and (31), we get

$$\phi = -\frac{\psi_c'''}{8\psi_c''} J + \text{h.o.t.} \tag{33}$$

Equation (31) implies that on the stabilized stall branch we must have $\psi < 0$, since $\psi_c'' < 0$ and $J > 0$, i.e., the stabilized stall branch always drops below the peak. If $\psi_c''' > 0$, i.e., the unstable (left) part of the characteristic is steeper than the stable (right) part of the characteristic, then we have $\phi > 0$ by equation (33), which means the stabilized stall branch tilts to the right of the characteristic. This back-tracking phenomenon is observed in our experiments (see Figure 17). On the other hand if $\psi_c''' < 0$, i.e., the unstable (left) part of the characteristic is shallower than the stable (right) part of the characteristic, then we have $\phi < 0$ by equation (33), which means the stabilized stall branch tilts to the left of the characteristic. This agrees the phenomena observed by Eveker *et al* (1995, 1998). It should be mentioned that the case $\psi_c''' > 0$ requires faster bleed valves than the case when $\psi_c''' < 0$ provided all other conditions are the same.

In all of the plots in Figure 18, the dashed line represents the one-to-one line between the theory- or simulations-predicted and experimentally obtained rate values. The minimum rate obtained through experiment is described in the previous section. The uncertainties associated with disturbance valve in the experiments is about three percent of throttle coefficient at the peak of the characteristic. So in the two formulas (25) and (27) we use three percent operability enhancement and solve for the rate. The rate obtained from the formulas are plotted against the rate obtained on the experiments in the first plot in Figure 18. Although the rate predicted by formulas is quantitatively different from that of the experiment, they give qualitatively the same trend. For example, the rate requirement order of expt5, expt2 and

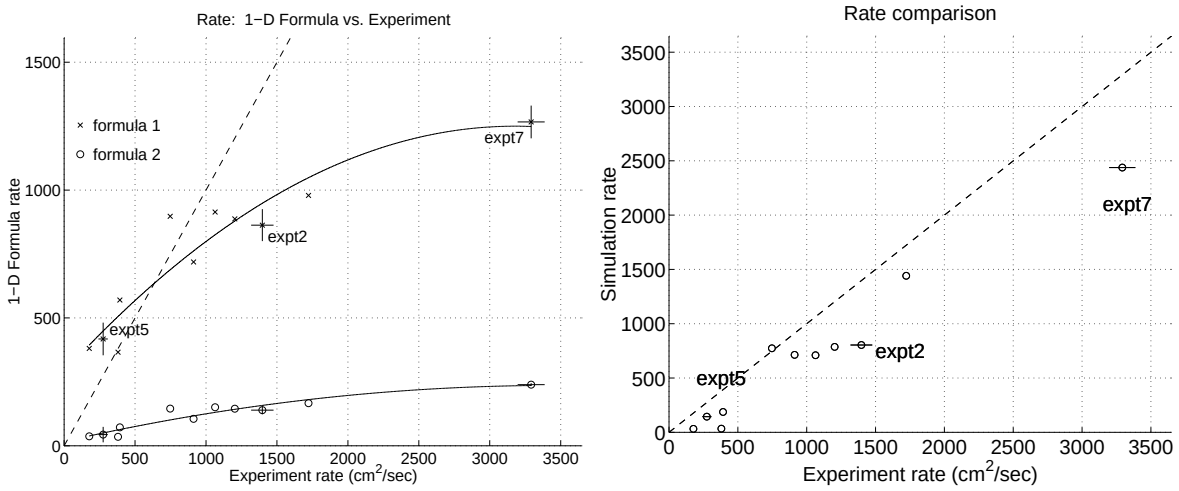

Figure 18: Comparison of rate predicted by theory, simulations of Mansoux model, and experiments. The bars in the x-direction indicate the standard deviation associated with the fluid- and human-induced error in computing the theoretical rate values (through identifying the unstable of $\Psi_c(\Phi)$ using surge cycle data), and the bars in the y-direction the standard deviation in the experimental values.

expt7 is consistent for both the experiment and the the theoretical formulas (see Figure 18). For the comparison results, it should be pointed out that the experiments show that the rate requirement for peak stabilization is reduced from approximately 145 Hz to below 10 Hz are reported by varying the amount of compressor characteristic actuation. Regarding the theoretical tools used for prediction, one can see from the figure that formula (25) seems to predict the rate requirement more accurately than formula (27). The main difference between the two expressions originates from the different ways an approximation to the solution to the stable manifold of the saddle S_1. The difference between the predictions of the two formulas has also been shown in Figure 13. Also, the difference between rate predictions by the formulas and the experiments becomes larger as the rate increases. The reason is that in the experiments, the rate was set as constraint so that the valve would not open or close faster than that. As the constraint relaxes (the rate increases), the valve hit the rate constraint during only part of the cycle, and is limited by bandwidth during the other part of the cycle. But the theoretical formulas assume the valve hits the rate limit all the time, and thus they predicted lower rate requirement. Nevertheless, both the formulas and experiments have predicted the same trend: the steeper the unstable part of the compressor characteristic near the peak, the more rate it requires. This can be seen from Figure 16 and Figure 18.

The values of rate predicted by simulations are plotted against the experimental values in Figure 18. It is not surprising that the rate estimates of the simulations match with the experimentally obtained counterpart more closely than the theoretical predictions (see second plot in Figure 18). One reason is that the Mansoux model is a much higher fidelity model than

either the three sate model or the reduced two dimensional model. Another reason is that it is easier to put the experimental criteria for peak stabilization ($\Phi \geq 0.9\Phi_0$ and $A \leq 0.5A_{\text{nom}}$) in the simulations.

6 Summary and Conclusions

The main conclusion is that actuator magnitude and rate limit is one of the critical issues that must be considered for practical implementation of bleed valve actuators in aircraft engines. High bandwidth and rate requirement for actuators in active control of rotating stall is due to the subcriticality of the Hopf bifurcation associated with stall inception: both the coefficients of linear and cubic terms in the dynamics on the center manifold are positive after the bifurcation. This nonlinear instability implies fast growth of stall once it is out of the linearly dominated region which may be under the noise level. We have demonstrated in this paper that the magnitude saturation level and rate limits of bleed severely restrict the robust performance of bleed valve actuators via models with different complexity: analytical studies on a lower order model, numerical simulations on a high fidelity model (37 states), and experiments on a low speed axial compressor. Since the low speed axial compressor in this paper may not be representative of the low and high speed compressors in a turbofan engine, it is necessary to carry out similar experiments on high speed compression systems representative of the engine, or even on an engine, to determine the quantitative tradeoffs between the actuator limits and operability enhancement.

Bifurcations and qualitative dynamics of the lower order model are analyzed via model reduction and phase plane analysis. The stable manifold of a saddle equilibrium is found critical for separating the trajectories that converge to the stabilized stall equilibrium and those converge to the fully developed stall equilibrium. By approximating this manifold, formulas have been derived for operability enhancement as explicit functions of the magnitude saturation level, rate limits, noise level, and the shape of the compressor characteristic. The formulas give good qualitative predictions of rate requirement when compared with the experiments and high fidelity simulations. The effects of time delay due to sensor bandwidth and filters are analyzed and found more detrimental to the control effectiveness, especially when the noise level is high and the compressor characteristic is steep near the peak.

As the major nonlinearity, the shape of compressor characteristic has a strong influence on robustness (or operability enhancement) of controllers. The rate requirement becomes more demanding when the curvature of the characteristic is large, and especially when the unstable part is steeper than the stable part. In experiments, a family of actuated compressor characteristics are obtained by varying the amount of continuous air injection on the system. The actuation provided by air injection makes the unstable part of the characteristic much shallower than the unactuated characteristic, thus drastic reduction of the rate requirements for bleed valve actuators are achieved. More details on the use of compressor characteristic actuation for the reduction of bleed valve rate requirement for control of rotating stall will be provided with the release of the patent by Yeung and Murray (1997).

For a compression system representative of aeroengines, any active control law must ad-

dress rotating stall and surge simultaneously. The theoretical studies on effects of noise and actuator limits in this case were presented in Wang and Murray (1998). The theory in this paper can also be applied to other actuation schemes such as air injectors (Yeung, 1998) and magnetic bearings (Wang *et al*, 1999).

Acknowledgment The authors would like to thank United Technologies Research Center (UTRC) for loan of the high speed bleed valve that is used to achieve the results reported in this paper. We would also thank Dr. Robert L. Behnken, Dr. Raffaello D'Andrea, and Dr. Briano D. Coller for many helpful discussions.

References

[1] Badmus, O. O., Chowdhury, S., Eveker, K. M., Nett, C. N., and Rivera, C. J. (1993). A simplified approach for control of rotating stall—part 2: experimental results. *29th Joint Propulsion Conference and Exhibit*, AIAA Paper #93-2234.

[2] Bansal, I., (1993). Advanced control for airbreathing engines - volume 2, General Electric Aircraft Engines. *U.S. Department of Commerce, National Technical Information Service*, N-9412271.

[3] Behnken, R. L. (1996). Nonlinear control and modeling of rotating stall in an axial flow compressor, *Ph.D thesis, California Institute of Technology.*

[4] Behnken, R. L., Leung, M., and Murray, R. M. (1997). Characterizing the effects of air injection on compressor performance for use in active control of rotating stall. *Proceedings of the International Gas Turbine and Aeroengine Congress and Exhibition*, ASME 97-GT-316.

[5] D'Andrea, R., Behnken, R. L., and Murray, R. M. (1998). Active control of an axial flow compressor via pulsed air injection. *ASME Journal of Turbomachinery* **119**(4), 742-752.

[6] Day, I. J. (1993). Active suppression of rotating stall and surge in axial compressors. *ASME Journal of Turbomachinery* **115**(1), 40-47.

[7] Eveker, K. M., Gysling, D. L., Nett, C. N., and Sharma, O. P. (1995). Integrated control of rotating stall and surge in aeroengines, *Sensing, Actuation, and Control in Aeropropulsion.* J. D. Paduano, Editor, Proc. SPIE 2494, 21-35.

[8] Eveker, K. M., Gysling, D. L., Nett, C. N., and Sharma, O. P. (1998). Integrated control of rotating stall and surge in high-speed multistage compression systems, *ASME Journal of Turbomachinery* **120**, 440-445.

[9] Freeman, C., Wilson, A. G., Day, I. J., and Swinbanks, M. A. (1998). Experiments in active control of stall on an aeroengine gas turbine. *ASME Journal of Turbomachinery* **120**, 637-647.

[10] Greitzer, E. M., 1981, "The Stability of Pumping Systems—The 1980 Freedman Scholar Lecture", *ASME Journal of Fluid Engineering*, Vol. 103, pp. 193-242.

[11] Greitzer, E. M., and Moore, F. K. (1986). A theory of post-stall transients in axial compression systems: part II—application. *ASME Journal of Engineering for Gas Turbines and Power* **108**(2), 231-240.

[12] Guckenheimer, J., and Holmes, P. (1983). *Nonlinear Oscillations, Dynamical Systems, and Bifurcations of Vector Fields*, Springer-Verlag, New York.

[13] Gysling, D. L., and Greitzer, E. M. (1994). Dynamic control of rotating stall in axial flow compressor using aeromechanical feedback. *ASME Journal of Turbomachinery* **117**(3), 307-319.

[14] Hendricks, G. J., and Gysling, P. L. (1994). Theoretical study of sensor-actuator schemes for rotating stall control. *Journal of Propulsion and Power* **10**(1), 101-109.

[15] Haynes, J. M., Hendricks, G. J., and Epstein, A. H., (1994). Active stabilization of rotating stall in a three-stage axial compressor. *Journal of Turbomachinery* **116**, 226-239.

[16] Leonessa, A., Chellaboina, V.-S., and Haddad W. M. (1997). Globally stabilizing controllers for multimode axial flow compressor models via equilibria-dependent Lyapunov functions. *Proc. IEEE International Conference on Control Applications*, 63-68.

[17] Liaw, D. C., and Abed, E. H. (1996). Control of compressor stall inception: a bifurcation-theoretic approach. *Automatica* **32**(1), 109-115.

[18] Mansoux, C. A., Gysling, D. L., Setiawan, J. D., and Paduano, J. D. (1994). Distributed nonlinear modeling and stability analysis of axial compressor stall and surge, *Proc. the American Control Conference*, 2305-2316.

[19] McCaughan, F. E. (1990). Bifurcation analysis of axial flow compressor stability. *SIAM Journal of Applied Mathematics* **50**(5), 1232-1253.

[20] Moore, F. K., and Greitzer, E. M. (1986). A theory of post-stall transients in axial compression systems: part I—development of equations. *ASME Journal of Engineering for Gas Turbines and Power* **108**(1), 68-76.

[21] Murray, R. M., Wembhoff, E. L., Kantner, M., Dmukauskas, T., and Winters, B. (1996). Sparrow reference manual, *California Institute of Technology.*

[22] Paduano, J. D., Epstein, A. H., Valavani, L., Longley, J. P., Greitzer, E. M., and Guenette, G. R. (1993). Active control of rotating stall in a low-speed axial compressor. *ASME Journal of Turbomachinery* **115**(1), 48-56.

[23] Ralph, J. A., (1993). Advanced control for airbreathing engines - volume 1, Pratt and Whitney. *U.S. Department of Commerce, National Technical Information Service*, N-9412270.

[24] Wang, H. H., and Krstić, M., (1997). Control of deep-hysteresis compressors under limited actuator bandwidth. *Proc. IEEE International Conference on Control Applications*, 657-662.

[25] Wang, Y., and Murray, R. M. (1998). Effects of the shape of compressor characteristics on actuator requirements for rotating stall control. *Proc. 1998 American Control Conference*, 4602-4607.

[26] Wang, Y., and Murray, R. M. (1998). Effects of noise and actuator limits on rotating stall and surge control. *Proceedings of 1998 IEEE Conference on Decision and Control*, 4602-4607.

[27] Wang, Y., Paduano, J. D., and Murray, R. M. (1999). Nonlinear control design for rotating stall with magnetic bearing actuators. *Proceedings of 1999 IEEE Conference on Control Applications*, 730-736.

[28] Weigl H., Paduano, J., Frechette L., Epstein A., and Greitzer E., (1998). Active stabilization of rotating stall and surge in a transonic single stage compressor. *Journal of Turbomachinery*, **120**, 625-636.

[29] Yeung, S., and Murray, R. M. (1997). Reduction of bleed valve rate requirements for control of rotating stall using continuous air injection. *Proc. IEEE International Conference on Control Applications*, 683-690.

[30] Yeung, S., and Murray, R. M. (1997). Actuator bandwidth and rate limit reduction for control of compressor rotating stall. *U. S. Patent Application, Serial No. 08/951,439.*

[31] Yeung, S. (1998). Nonlinear control of rotating stall and surge with axisymmetric bleed and air injection on axial flow compressors. *Ph.D thesis, California Institute of Technology.*

A The proof of Proposition 3.1 and Proposition 4.1

A.1 Proof of Proposition 3.1

We give a sketch of proof to Proposition 3.1. We assume the compressor characteristic $\psi_c(\cdot)$ is an analytic function, i.e., the Taylor series of expansion of $\psi_c(\Phi + x)$ is convergent for any Φ. So

$$\psi_c(\Phi + x) = \sum_{k=0}^{\infty} \frac{\psi_c^{(k)}(\Phi)}{k!} x^k.$$

Now, by substituting the Taylor series expansion into the three state Moore-Greitzer model (1), we get

$$\begin{aligned}
\frac{d\Phi}{d\xi} &= \frac{1}{l_c}\left(-\Psi + \psi_c(\Phi) + \sum_{k=1}^{\infty} \frac{\psi_c^{(2k)}(\Phi)}{[(2k)!!]^2} J^k\right) \\
\frac{d\Psi}{d\xi} &= \frac{1}{4B^2 l_c}\left(\Phi - (\gamma + u)\sqrt{\Psi}\right) \\
\frac{dJ}{d\xi} &= \frac{4}{m+\mu} \sum_{k=1}^{\infty} \frac{2k\psi_c^{(2k-1)}(\Phi)}{[(2k)!!]^2} J^k
\end{aligned} \tag{34}$$

where $J := A^2$. From Figure 7 and 8 we know in different regions of the u-J plane the control law has different forms:

(1) The bandwidth limit form: $u = \frac{KJ-u}{\tau}$, and $u = \frac{u_{mag}-u}{\tau}$.

(2) The rate limit form $u = \pm u_{rate}$.

(3) The magnitude limit form $u = u_{mag}$.

We first consider the case when $\dot{u} = \frac{KJ-u}{\tau}$. Letting

$$\begin{aligned}
&\phi = \Phi - \Phi_0, \quad \psi = \Psi - \Psi_0, \\
&v = u - KJ, \quad \delta = \gamma - \gamma_0.
\end{aligned}$$

Using Taylor series expansion, the system becomes

$$\begin{aligned}
\dot{J} &= \frac{1}{m+\mu}\left(2\psi_c''\phi J + \frac{\psi_c'''}{4} J^2\right) + \text{h.o.t.} \\
\dot{\phi} &= \frac{\psi_c''}{4l_c} J - \frac{1}{l_c}\psi + \frac{1}{l_c}\left(\frac{\psi_c''}{2}\phi^2 + \frac{\psi_c'''}{4}\phi J + \frac{\psi_c^{(4)}}{64} J^2\right) + \text{h.o.t.} \\
\dot{\psi} &= -\frac{\sqrt{\Psi_0}K}{4B^2 l_c} J + \frac{1}{4B^2 l_c}\phi - \frac{\gamma_0}{8B^2 l_c\sqrt{\Psi_0}}\psi - \frac{\sqrt{\Psi_0}}{4B^2 l_c} v - \frac{\sqrt{\Psi_0}}{4B^2 l_c}\delta \\
&\quad -\frac{1}{8B^2 l_c\sqrt{\Psi_0}}\left(\psi v + K\psi J - \frac{\gamma_0}{4\Psi_0}\psi^2\right) + \text{h.o.t.} \\
\dot{v} &= -\frac{1}{\tau} v + \frac{K}{m+\mu}\left(2\psi_c''\phi J + \frac{\psi_c'''}{4} J^2\right) + \text{h.o.t.}
\end{aligned}$$

Since $\tau > 0$ and B is small, the system possesses a three dimensional stable manifold and a one dimensional center manifold. Let

$$\begin{aligned}
\phi &= \beta_{11}\delta + \beta_{12} J + \mathcal{O}\left(\delta^2, \delta J, J^2\right), \\
\psi &= \beta_{21}\delta + \beta_{22} J + \mathcal{O}\left(\delta^2, \delta J, J^2\right), \\
v &= \beta_{31}\delta + \beta_{32} J + \mathcal{O}\left(\delta^2, \delta J, J^2\right).
\end{aligned}$$

By differentiating these equalities and using the systems equations, we get

$$\begin{array}{lll} \beta_{11} = \sqrt{\Psi_0}, & \beta_{21} = 0, & \beta_{31} = 0, \\ \beta_{12} = \sqrt{\Psi_0}\ K + \frac{\gamma_0 \psi_c''}{8\sqrt{\Psi_0}}, & \beta_{22} = \frac{\psi_c''}{4}, & \beta_{32} = 0. \end{array}$$

So the dynamics on the center manifold is given by

$$\begin{aligned} \dot{J} &= \frac{1}{m+\mu}\left(2\psi_c''\phi J + \frac{\psi_c'''}{4}J^2\right) + \text{h.o.t.} \\ &= \alpha_1(\delta + KJ)J + \alpha_2 J^2 + \text{h.o.t.} \\ &= \alpha_1(\delta + u)J + \alpha_2 J^2 + \text{h.o.t.} \end{aligned}$$

The last equality holds because $u = v + KJ$ and $v = \mathcal{O}\left(\delta^2, \delta J, J^2\right)$. So the reduced system is given by

$$\begin{aligned} \dot{J} &= \alpha_1(\delta + u)J + \alpha_2 J^2 + \text{h.o.t.}, \\ \dot{u} &= \frac{KJ - u}{\tau}, \end{aligned} \tag{35}$$

where α_1 and α_2 are given by (6) and (7).

For other types of control laws, similar procedure could be followed. The resulting reduced system is the same as (35), together with the actuator dynamics. It should be mentioned that for the case when $\dot{u} = \pm u_{rate}$, the reduction is no longer a center manifold reduction, but rather an approximation of the ϕ and ψ variables using J and δ. The proof is done by combining all these cases.

A.2 Proof of Proposition 4.1

Consider the three state Moore-Greitzer model (34) with control input $u(\xi)$. Letting

$$\phi = \Phi - \Phi_0, \quad \psi = \Psi - \Psi_0, \quad \delta = \gamma - \gamma_0,$$

Then (34) is transformed to

$$\begin{aligned} \dot{J} &= \frac{1}{m+\mu}\left(2\psi_c''\phi J + \frac{\psi_c'''}{4}J^2\right) + \text{h.o.t.} \\ \dot{\phi} &= \frac{\psi_c''}{4l_c}J - \frac{1}{l_c}\psi + \frac{1}{l_c}\left(\frac{\psi_c''}{2}\phi^2 + \frac{\psi_c'''}{4}\phi J + \frac{\psi_c^{(4)}}{64}J^2\right) + \text{h.o.t.} \\ \dot{\psi} &= \frac{1}{4B^2 l_c}\phi - \frac{\gamma_0}{8B^2 l_c\sqrt{\Psi_0}}\psi - \frac{\sqrt{\Psi_0}}{4B^2 l_c}u(\xi) - \frac{\sqrt{\Psi_0}}{4B^2 l_c}\delta \\ &\quad - \frac{1}{8B^2 l_c\sqrt{\Psi_0}}\left(\psi u(\xi) - \frac{\gamma_0}{4\Psi_0}\psi^2\right) + \text{h.o.t.} \end{aligned}$$

Now assume B is small so the axisymmetric dynamics is stable. Also assume the initial conditions for (ϕ, ψ) are small. Let

$$\begin{aligned} \phi &= \beta_{11}\delta + \beta_{12}J + \beta_{13}u + \text{h.o.t.}, \\ \psi &= \beta_{21}\delta + \beta_{22}J + \beta_{23}u + \text{h.o.t.}. \end{aligned}$$

By differentiating these equalities and use the system dynamics, we get

$$\begin{array}{lll} \beta_{11} = \sqrt{\Psi_0}, & \beta_{12} = \sqrt{\Psi_0}\ K + \frac{\gamma_0 \psi_c''}{8\sqrt{\Psi_0}}, & \beta_{13} = \sqrt{\Psi_0}, \\ \beta_{21} = 0, & \beta_{22} = \frac{\psi_c''}{4}, & \beta_{23} = 0. \end{array}$$

So the dynamics of the reduced system is given by

$$\dot{J} = \alpha_1(\delta + u)J + \alpha_2 J^2 + \text{h.o.t.}.$$

Using the procedure to match the hysteresis loop and the growth rate of stall at the bifurcation point, we get

$$\dot{J} = \alpha J \left(\alpha_1(\delta + u) + \sum_{k=2}^{n} \alpha_k J^{k-1} \right).$$

B A sketch of the proof of Theorem 4.1

The key figure for the proof is Figure 19. The reduced system with bang-on control is given by

$$\begin{aligned} \dot{J} &= \alpha \left[\alpha_1(\delta + u) + h(J) \right] J, \\ \dot{u} &= \begin{cases} 0 & \text{if } J \le J_{thresh}, \text{ or } J > J_{thresh} \text{ and } u = u_{mag}, \\ u_{rate} & \text{if } J > J_{thresh} \text{ and } 0 \le u < u_{mag}, \end{cases} \end{aligned}$$

where $h(J) = \sum_{k=2}^{n} \alpha_k J^{k-1}$, and $J_{thresh} = \epsilon$. It is easy to see that the curve $\dot{J} = 0$ is given by the curve S_E:

$$S_e \ : \ u = -\delta - \frac{1}{\alpha_1} h(J).$$

From the assumptions (A1) and (A2), the shape and location of $\dot{J} = 0$ is the dash-dot line in Figure 19. Assume $u_{mag} > -\delta$, then the curve S_E intersects the saturation line $u = u_{mag}$ at two points S_1 and S_2: S_1 is a saddle and S_2 is a sink. The shaded regions in Figure 19 satisfy $\dot{J} < 0$. Let $W^s(S_1)$ be the stable manifold of S_1. It is easy to prove that $W^s(S_1)$ must be in the region $\dot{J} > 0$. Or in other words, on $W^s(S_1)$, we have $\dot{J} > 0$. It is also clear that the

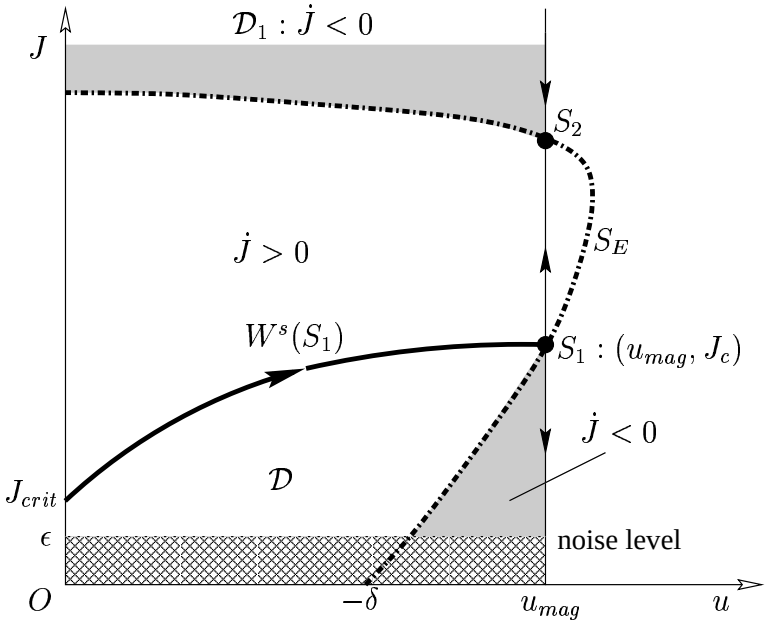

Figure 19: Key figure for the proof of Lemma A.1

trajectories under $W^s(S_1)$ denoted by $\mathcal{D}$ will remain in $\mathcal{D}$. Let $\mathcal{A}_\delta = \{J \mid 0 \le J \le J_c(\delta)\}$, it is clear that the region $\mathcal{D}$ is $\mathcal{A}_\delta$ attractive, i.e., all the trajectories in $\mathcal{D}$ satisfy $J(\xi) \le J_c(\delta)$ for any $\xi \ge 0$. Since the noise set is $\mathcal{E} = \{J \mid 0 \le J \le \epsilon\}$, the operability boundary for the bang-on control denoted by $\Delta(u, \mathcal{E})$ satisfies $J_{crit}(\Delta) = \epsilon$, where J_{crit} is the intersection of $W^s(S_1)$ and $u = 0$.

Now fix $\delta = \Delta(u, \mathcal{E})$, and let

$$v \in \mathcal{U} := \{u \mid 0 \le u \le u_{mag}, |\dot{u}| \le u_{rate}, u \text{ is piecewise smooth}\}$$

be any control law with magnitude limit u_{mag} and rate limits $\pm u_{rate}$. Let (u_1, J_1) be a point on $W^s(S_1)$, then for the reduced system we have

$$\dot{J}\Big|_v = \dot{J}\Big|_u, \quad \dot{v} \le \dot{u} = u_{rate}, \tag{36}$$

where $\dot{J}\Big|_v$ is $\dot{J}$ with control input $v(\xi)$, and $\dot{J}\Big|_u$ is $\dot{J}$ with control input $v(\xi)$. Relations in (36) implies that the vector field for control input $v(\xi)$ on $W^s(S_1)$ point to the outside of $\mathcal{D}$. In other words, each trajectory for control $v(\xi)$ with initial condition $(0, J_{crit})$ satisfying $J_{crit} > \epsilon$ will not enter region $\mathcal{D}$, and will eventually intersects with S_E since the trajectory is either in the region $\dot{J} > 0$, or in the region $\mathcal{D}_1$ with $\dot{J} < 0$ (see Figure 19). So the operability boundary for control input $v(\xi)$ denoted by $\Delta(v, \mathcal{E})$ satisfies

$$\Delta(v, \mathcal{E}) \ge \Delta(u, \mathcal{E}).$$

The fact that ϵ is th worst noise is clear since if a trajectory for the bang-on control input u with initial condition $(u, J) = (0, J_0)$ $(J_0 \leq \epsilon)$ converges to the fully developed stall equilibrium S_2, i.e., $(0, J_0)$ is not $\mathcal{A}_\delta$ attractive, then then we must have $J_0 > J_{crit}$ (see Figure 19). So $\epsilon \geq J > J_{crit}$, and the trajectory with initial condition $(u, J) = (0, \epsilon)$ will also converge to S_2, i.e., $(0, \epsilon)$ is not $\mathcal{A}_\delta$ attractive.

We remark here that control laws in $\mathcal{U}$ might create equilibria or limit cycles for the controlled system. But Theorem 4.1 only claims that it is the bang-on control law that prevents more trajectories going to the fully developed stall equilibrium.